arXiv:cond-mat/0407627v2 [cond-mat.other] 10 Feb 2005

Ramsey interferometry with atoms and molecules: two-body versus many-body phenomena

Krzysztof Góral,[1,2] Thorsten Köhler,[1] and Keith Burnett[1]
[1]Clarendon Laboratory, Department of Physics, University of Oxford, Parks Road, Oxford, OX1 3PU, United Kingdom
[2]Center for Theoretical Physics, Polish Academy of Sciences, Aleja Lotników 32/46, 02-668 Warsaw, Poland

(Dated: February 2, 2008)

We discuss the frequency and visibility of atom-molecule Ramsey fringes observed in recent experiments by Claussen *et al.* [Phys. Rev. A **67**, 060701 (2003)]. In these experiments a ^{85}Rb Bose-Einstein condensate was exposed to a sequence of magnetic field pulses on the high field side of the 155 G Feshbach resonance. The observed oscillation frequencies largely agree with the theoretically predicted magnetic field dependence of the binding energy of the highest excited diatomic vibrational state, except for a small region very close to the singularity of the scattering length. Our analytic treatment of the experiment, as well as our dynamical simulations, follow the magnitude of the measured oscillation frequencies as well as the visibilities of the Ramsey fringes. We show that significant deviations from a purely binary dynamics, with an associated binding frequency, occur when the spatial extent of the molecular wave function becomes comparable with the mean distance between the atoms in the dilute gas. The experiments thus clearly identify the conditions under which diatomic molecules may be identified as a separate entity of the gas or, conversely, when the concept of binary physics in a many-body environment is bound to break down.

PACS numbers: 03.75.Kk, 34.50.-s, 05.30.-d

I. INTRODUCTION

The study of ultra-cold molecules produced in atomic Bose and Fermi gases is one of the most important developments in cold atom physics [1]. One of the most successful experimental techniques to produce molecules in atomic Bose-Einstein condensates utilised adiabatic sweeps of a magnetic field tunable Feshbach resonance level across the zero energy threshold of the colliding atoms, during which a highly excited diatomic vibrational bound state could be efficiently populated [2, 3, 4, 5, 6]. In this paper we study a coherent superposition of an atomic condensate and molecules. The production of such a coherent superposition in a degenerate gas of bosons, demonstrated in Refs. [7, 8], is a remarkable achievement, given the marked difference in the relevant energy and time scales for condensates and molecules. These experiments employed a sequence of two magnetic field pulses each of which rapidly approached the position of the zero energy resonance (the magnetic field strength at which the scattering length has a singularity) on the side supporting the highly excited diatomic vibrational bound state. The two pulses were separated by an evolution period of variable duration as a function of which the oscillations in the final condensate populations were observed. This achievement offers the possibility of precise interferometric measurements of the energies of the relevant states through the measurement of bulk properties of the gas. It is the theory of such measurements we present in this paper.

We set up the theory in a way that reflects properly the analogy with Ramsey – separated pulse – interferometers with the splitting and recombination occurring during the magnetic field pulses at the beginning and the end of the magnetic field sequence, respectively. We give a complementary account of the experiment which emphasises the interferometer picture and will, we believe, be of greater utility to those analysing experiments than just the simulation on its own can do.

To provide a simple intuitive physical description of the experiments, we first consider the evolution of a single pair of cold trapped atoms subjected to the experimental pulse sequence. We show that the first pulse splits the initial state of the pair into three different components (interferometer arms). The bound state component evolves most quickly. The other components are a superposition of excited quasi continuum states and the lowest energetic quasi continuum state, which are the two-body analogues of the experimentally observed [7] burst of atoms and the remnant Bose-Einstein condensate, respectively. After a variable period of time, referred to as the evolution period, during which the bound and free states evolve almost independently, the second pulse recombines the components. The final state of the pair depends sensitively on the phase differences built up between the amplitudes of the various components during the evolution period. As a consequence, oscillations in the resulting populations of the three components of the pair wave function are observed as the time between the pulses is varied. We shall show that the oscillation frequency is determined by the energy of the molecular bound state populated in the process. The visibility of these oscillations, i.e. Ramsey fringes, depends on both the efficiency of populating the bound state during the first pulse and of dissociating the molecules during the second pulse of the sequence. We observe that these quantities are very sensitive to both the details of the underlying two-body physics and the precise duration and shape of the pulses. We provide analytic estimates of the molecular production and dissociation efficiencies and give an analogy between the function of the pulses and the concept of two colour photo-association of molecules.

We extend this description of a single pair of atoms in order to apply it to a gas of atoms by using a coarse graining procedure. In this approach the populations of the different components of the gas are obtained, following classical probability theory, by averaging over the microscopic transition probabilities for all pairs. We show that this straightforward but systematic extension of the two-body physics recovers the experimental observations rather well, in terms of the oscillation frequency, the amplitude and the relative populations of all three components present in the gas.

In order to disentangle the two-body and many-body aspects of Ramsey interferometry with cold gases, we have also used the genuinely many-body microscopic quantum dynamics approach to the dynamics of partly condensed Bose gases [9, 10]. We base our full simulations on the non-Markovian non-linear Schrödinger equation of the first order microscopic quantum dynamics approach. This equation describes the evolution of the condensate along with the dynamics of pair correlations. The method describes fully and quantitatively the evolution of the states produced by magnetic pulse shape induced rapid changes in the Hamiltonian describing the inter-atomic potential. In particular, the microscopic quantum dynamics approach incorporates the entire binary collision dynamics in a non-perturbative manner.

We shall see that the many-body phenomena affect both the frequency and visibility of the Ramsey fringes. In the first step in this direction, we have found an analytical solution of the non-Markovian equation using a perturbative approximation. In agreement with the experimental observations, we show that the frequencies of the Ramsey fringes are shifted upwards with respect to the value associated with the energy of the weakly bound molecular state populated in the process. This shift persists for all values of the magnetic field, it does, however, become hard to discern above B_{evolve} (the value of the magnetic field strength between the pulses) higher than roughly 158 G. Away from the zero energy resonance the shift is given, as one might reasonably expect, by roughly twice the chemical potential. The shift is typically a small correction to the oscillation frequency, and a time scale much longer than the typical pulse durations of the experiments [8] would be required for it to be fully resolved. The visibility of the Ramsey fringes is reduced in comparison with the two-body result due to the non-linear dynamics of the atomic condensate mean field.

Our analytic studies apply when the experiments [7, 8] are operated in what we shall term the "interferometer mode", i.e. when the magnetic field strength B_{evolve} during the evolution period is sufficiently far away from the zero energy resonance for two- and many-body phenomena to be disentangled. In this regime of magnetic field strengths B_{evolve} the gas is weakly interacting during the evolution period and no significant population exchange between the bound and unbound components occurs. The different components are then orthogonal as they should be in an ideal Ramsey interferometer. Claussen *et al*. [8] also performed measurements in the close vicinity of the zero energy resonance, where the gas is subject to a non-equilibrium dynamics even between the pulses. For all experimentally studied cases we have performed full simulations of the non-Markovian equation for the trap geometry and atom number employed in the experiments. In the regime very close to the zero energy resonance the non-linear aspects of the dynamics are especially significant, and the description of the experiment in terms of an ideal Ramsey interferometer is not as clear, because the three components of the gas are no longer orthogonal. The full numerical simulation does not rely on this assumption and is, therefore, essential in the comparison with experimental data for this regime. We should emphasise that in this region the idea that we can clearly separate molecules and atoms is also breaking down as the spatial extent of the molecular bound state wave function approaches the mean distance between the atoms in the gas [11]. This makes the simple picture invalid as well as any theory that relies on such a distinction.

One might be misled in this analysis if one focused purely on the component of the molecular bound state in the bare resonance level that remains, of course, very small in extent. Our analysis shows, for instance, that the frequently used two level mean field approach of Refs. [12, 13, 14, 15, 16, 17, 18], fails entirely to describe the interferometric experiments of Refs. [7, 8], despite the fact that it can provide accurate predictions on the final molecular fractions in Feshbach resonance crossing experiments [19, 20]. In Ref. [21] a modified two level mean field approach was applied to the observations of Ref. [8], in which the energy of the bare Feshbach resonance level was tuned to recover the binding energy of the molecules produced in the experiments [7, 8]. This approach recovered the magnitude of the fringe frequencies of Ref. [8] after adjusting the densities used in the theory. We believe, however, that such a treatment is inconsistent because any two level approach crucially lacks the excited energy levels of the background scattering continuum [20]. This treatment obviously leads to the absence of the experimentally observed burst component of atoms [7] in the theory. The two level approach of Ref. [21] also inevitably misrepresents the molecular bound state [22] produced in the experiments [8], as this bound state is even dominated by its component in the background scattering continuum.

The Ramsey fringes predicted by our dynamical simulations of the non-Markovian equation recover all the systematic trends observed in the experiment. For magnetic fields away from the zero energy resonance, the Ramsey fringes are essentially undamped on the comparatively short time scales of the pulse sequences and their frequencies are only slightly shifted with respect to the value determined from the energy of the weakly bound molecular state. Closer to the zero energy resonance, a significant decoherence of the Ramsey fringes has been observed in the experiment, a feature also predicted by our many-body approach. We also recover the substantial upward shift of the fringe frequencies for the magnetic field strengths closest to the zero energy resonance, for which the shift was attributed in Ref. [8, 23]. We show that this shift can be interpreted in terms of a measure of the extent to which diatomic molecules in the highly excited vibrational state can be considered as a separate entity of the gas. Our studies also strongly indicate that the significant experimentally [8] observed loss of condensate atoms, which is particularly clear for longer pulse sequences with the magnetic field strength B_{evolve} in the close vicinity of the zero energy resonance, is essentially determined by the same parameters of the binary interactions that determine the frequency and visibility of the fringe pattern. This observation implies that deeply inelastic loss phenomena such as resonance enhanced spin relaxation of ^{85}Rb atoms [24], are unlikely to play a significant role in the experiments [7, 8].

Both the two-body and many-body pictures presented in this paper reveal the remarkable sensitivity of these experiments to the details of the underlying two-body physics, details that are clouded over in experiments involving molecular production using linear crossing of a Feshbach resonance [19, 20]. The interferometric technique, therefore, offers a rather unique probe of the microscopic collision physics through observing the macroscopic bulk properties of the gas.

II. PHYSICAL ORIGIN OF THE RAMSEY FRINGES

In this section we provide a physical explanation for the experimental fringe patterns reported in Refs. [7, 8] in terms of general properties of a Ramsey interferometer. We then provide a very direct determination of the frequency and visibility of the Ramsey fringes in terms of the dynamics of a single pair of atoms. We then present the first order many-body corrections to the frequency and visibility obtained from the microscopic quantum dynamics approach of Refs. [9, 10]. This allows us to distinguish pure two-body contributions to the interference between atoms and molecules from many-body phenomena related to the coherent nature of the partially condensed Bose gas.

A. Atom-molecule coherence in a Bose-Einstein condensate

In the experiments of Refs. [7, 8] a Bose-Einstein condensate of ^{85}Rb atoms in the $(F = 2, m_F = -2)$ hyperfine state was exposed to a sequence of spatially homogeneous magnetic field pulses on the high field side of the 155 G Feshbach resonance. A typical pulse sequence [25] is depicted in Fig. 1. The pulses, at the beginning (#1) and the end (#2) of the sequence, each consisted of linear downward and then upward ramps, which were separated by a hold period of constant magnetic field strength, close to the position of the zero energy resonance at $B_0 = 155.041$ G [8]. The evolution period of constant magnetic field strength $B_{\rm evolve}$ separated the pulses by an amount of time $t_{\rm evolve}$. In the course of the experiments [7, 8], the final densities of atoms were recorded after expanding the cloud, and the measurements were repeated with variable evolution times $t_{\rm evolve}$ and magnetic field strengths $B_{\rm evolve}$.

1. Interference between different components of a partially condensed Bose gas

Donley *et al.* [7] have identified two different components of the final atomic cloud: a remnant Bose-Einstein condensate and a burst of atoms with a comparatively high mean kinetic energy of roughly $E_{\rm kin}/k_B = 150$ nK ($k_B = 1.3806505 \times 10^{-23}$ J/K is the Boltzmann constant). The magnitudes of the burst and remnant condensate fractions exhibited an oscillatory dependence on the evolution time $t_{\rm evolve}$ of the magnetic field pulse sequence. The existence of a third component of missing atoms was inferred from the difference between the initial and total final numbers of detectable atoms. Donley *et al.* [7] suggested that the missing atoms indicated molecular production, and the oscillations were interpreted in terms of an interference between atoms and molecules during the evolution period of the pulse sequence.

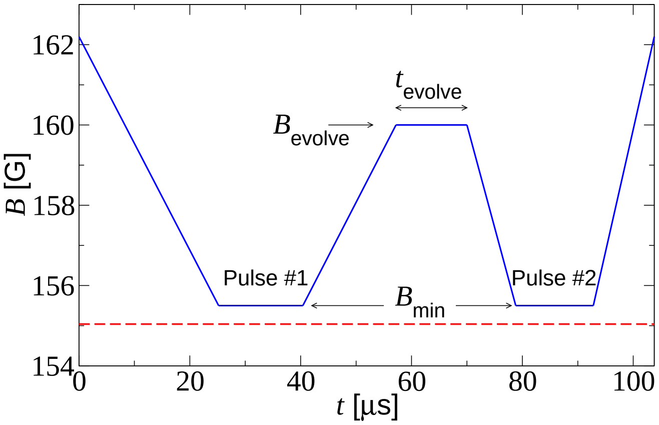

FIG. 1: A typical sequence of magnetic field pulses (solid lines) applied in the interferometric experiments of Refs. [7, 8]. The magnetic field strength at the minimum of the pulses #1 and #2 of $B_{\rm min} = 155.5$ G is closest to the zero energy resonance at $B_0 = 155.041$ G [8] (dashed, horizontal line), and leads to large positive scattering lengths on the order of 10000 $a_{\rm Bohr}$ ($a_{\rm Bohr} = 0.052918$ nm is the Bohr radius). The variable magnetic field strength and duration of the evolution period of the pulse sequence are denoted by $B_{\rm evolve}$ and $t_{\rm evolve}$, respectively.

This interpretation has been confirmed by subsequent theoretical studies [10, 26, 27]. Figure 2 shows a theoretical prediction of the final densities of atoms versus $t_{\rm evolve}$ for the pulse sequences and the initial conditions corresponding to Fig. 6 of Ref. [7]. The predictions in Fig. 2 were obtained from the microscopic quantum dynamics approach to dilute Bose-Einstein condensates [10, 28]. This gives a fringe pattern which compares rather favourably in both its qualitative and quantitative features with the observations reported in Ref. [7]. The same theoretical approach also recovers the experimentally observed kinetic energy of the burst atoms on the order of $k_B\times150$ nK [10].

2. The different regimes of molecular vibrational frequencies

The frequencies of the fringes have been identified as the vibrational frequencies of the highest excited diatomic vibrational bound state $\phi_b(B_{\rm evolve})$ at the magnetic field strength $B_{\rm evolve}$ of the evolution period [7], through their remarkable agreement with the result of coupled channels calculations (cf. Fig. 3). The marked magnetic field dependence of the binding energy $E_b(B_{\rm evolve})$ associated with the bound state $\phi_b(B_{\rm evolve})$ is depicted in Fig. 3. We note that the range of frequencies measured via bulk properties of the gas extends over three orders of magnitude from several kHz to the MHz regime. The associated oscillation periods are very much

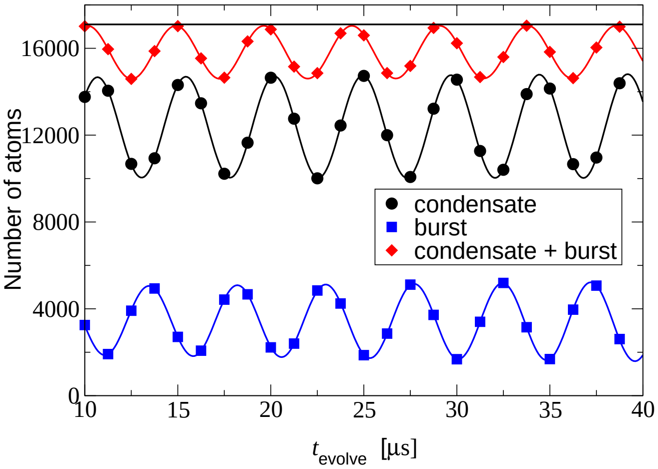

FIG. 2: Predicted numbers of condensate and burst atoms at the end of the magnetic field pulse sequence as a function of t_{evolve} for a magnetic field strength of $B_{\text{evolve}} = 159.84$ G in the evolution period of the pulse sequence. The total number of atoms is 17100 (horizontal line). The predictions were obtained from numerical solutions of the non Markovian non-linear Schrödinger equation (28), including a fully quantum mechanical description of the inhomogeneity of the gas [28] and a two-channel description of the low energy binary collision dynamics. The magnetic field pulse sequence (cf. Fig. 1), trap frequencies, and initial ground state condensate densities correspond to the measurements in Fig. 6 of Ref. [7].

shorter than typical time scales set by the bulk motion of dilute Bose-Einstein condensates, which are typically on the order of the trap period of about 1/10 of a second in Refs. [7, 8].

For the regime of the high MHz oscillation frequencies the spatial extent of the molecular wave function is typically on the order of several nanometres [11], while the length scale of the atomic cloud is set by the trap length of about 3000 nm. In view of these enormous differences in the orders of magnitude the visibility of the Ramsey fringes is a remarkable phenomenon in its own right. In the opposite regime of low kHz oscillation frequencies, i.e. very close to the zero energy resonance at $B_0 = 155.041$ G, Claussen *et al.* [8] have observed pronounced upward shifts of the fringe frequencies with respect to the vibrational frequencies of the molecules. The frequency shifts were accompanied by a strong damping of the fringe pattern. This damping suggests an enhancement of the influence of many-body phenomena related to the coherent nature of the dilute Bose-Einstein condensate on the fringe pattern, as the magnetic field strength approaches the zero energy resonance.

B. Ramsey interferometry with atoms and molecules in a Bose-Einstein condensate

We shall now identify the different elements of a Ramsey interferometer from the pulse sequence in Fig. 1. Our analysis will show that in the regime of comparatively high molecular vibrational frequencies the atom-molecule oscillation experiment [7, 8] can be directly interpreted in terms of Ramsey interferometry, while in the opposite low frequency regime a loss of coherence is expected to wipe out the fringes.

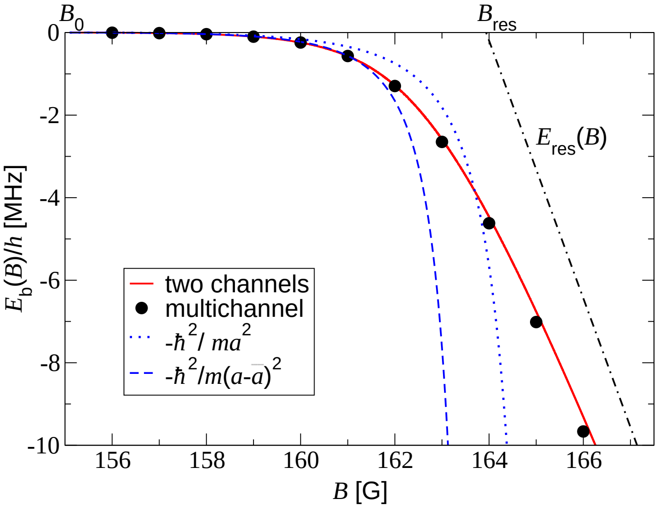

FIG. 3: Binding energy $E_b(B)$ of the highest exited vibrational molecular bound state $\phi_b(B)$ of two ^{85}Rb atoms in dependence on the magnetic field strength B. The figure shows comparisons between full coupled channels calculations [8, 29] (circles), the two channel approach of Refs. [19, 20] (solid curve), and single channel analytic estimates [10] of the binding energy (dotted and dashed curves) in the vicinity of the zero energy resonance at $B_0 = 155.041$ G. While the dotted curve refers to the universal estimate, just depending on the scattering length a, the dashed curve also accounts for the van der Waals interaction $-C_6/r^6$, at large inter-atomic distances r, in terms of the mean scattering length $\bar{a}$ [10, 30]. The dotted-dashed line indicates the linear dependence of the energy $E_{\text{res}}(B)$, associated with the Feshbach resonance level $\phi_{\text{res}}(r)$, on the magnetic field strength. Here and throughout this paper, we have chosen the zero of the energy, at each magnetic field strength B, as the energy of two asymptotically free ^{85}Rb atoms in the $(F = 2, m_F = -2)$ state.

1. *Interpretation of the magnetic field pulses in terms of beam splitters*

We shall first show that the pulses #1 and #2 of Fig. 1 provide the analogue of beam splitters through rapid tuning of the inter-atomic forces in the gas between the weakly and the strongly interacting regime. This is achieved by the variation of the scattering length $a(B)$, which characterises the static binary interactions in dilute Bose-Einstein condensates and depends on the magnetic field strength B in accordance with the formula:

$$a(B) = a_{\text{bg}}\left(1 - \frac{\Delta B}{B - B_0}\right). \tag{1}$$

Here $a_{\text{bg}} = -443\, a_{\text{Bohr}}$ ($a_{\text{Bohr}} = 0.052918$ nm is the Bohr radius) and $\Delta B = 10.71$ G [8] are the background scattering length and the resonance width, respectively. At the minimum of the magnetic field pulses the stationary magnetic field strength of $B_{\mathrm{min}} = 155.5$ G thus implies a large positive scattering length of about 10000 a_{Bohr}, which is close to the mean inter-atomic distance of about 12000 a_{Bohr} in the dilute gas. The singularity of the scattering length in Eq. (1) is a decisive feature of all zero energy resonances in ultra-cold collision physics and indicates the emergence of a highly excited diatomic vibrational bound state $\phi_{\mathrm{b}}(B)$ at the magnetic field strength B_0 of the zero energy resonance. This molecular bound state exists just on the side of positive scattering lengths (cf. Fig. 3), and its mean internuclear distance is largely determined by $\langle r \rangle = a(B)/2$ [11, 31].

The favourable overlap between the diatomic energy states and the many-body state of the gas provides the necessary conditions for producing the desired strongly correlated pairs of atoms in the molecular bound state $\phi_{\mathrm{b}}(B_{\mathrm{evolve}})$, during the upward ramp at the end of the first magnetic field pulse. The association of bound molecules at the final magnetic field strength B_{evolve} of Pulse #1 is accompanied by the production of correlated pairs of atoms in the continuum of positive energies above the two-body dissociation threshold. The occupation of these continuum states provides a first burst component that diffuses during the evolution period. The first magnetic field pulse thus splits the virtually uncorrelated initial Bose-Einstein condensate into three components; the remnant Bose-Einstein condensate, bound molecules and burst atoms.

2. *The evolution period*

In the ideal limit of coherent Ramsey interferometry, the gas is weakly interacting during the evolution period, i.e. B_{evolve} is sufficiently far from the zero energy resonance that the scattering length $a(B)$ is much smaller than the mean distance between the atoms in the dilute gas. The remnant condensate, burst and bound molecular components are then virtually orthogonal and evolve coherently. The amplitude of the molecular component in the state $\phi_{\mathrm{b}}(B_{\mathrm{evolve}})$ thus acquires a phase shift of $\Delta\varphi = |E_{\mathrm{b}}(B_{\mathrm{evolve}})|t_{\mathrm{evolve}}/\hbar$ (cf. Fig. 3) relative to the slowly varying amplitudes of the burst and condensate components.

3. *The second magnetic field pulse*

The second magnetic field pulse gets all three components to overlap and thereby probes the phase differences between their amplitudes. The final densities of the three components are therefore sensitive to the phases of their amplitudes at the end of the evolution period, which explains the emergence of a fringe pattern as a function of t_{evolve} as well as its angular oscillation frequency of $\omega_{\mathrm{e}} = |E_{\mathrm{b}}(B_{\mathrm{evolve}})|/\hbar$.

We note that in order to observe coherent Ramsey fringes, the different components of the system need to be orthogonal during the evolution period. In Ramsey interferometers with light or atomic beams the beam splitters provide the spatially separated, i.e. orthogonal, components. In the atom-molecule coherence experiment orthogonality is provided by the ideally large difference in the orders of magnitude between the mean inter-atomic distance in the atomic burst and condensate components on one hand and the comparatively small bond length of the bound molecules during the evolution period on the other hand. In both cases the lack of overlap prevents any significant exchange between the components during the evolution period.

C. Frequency and visibility of the interference fringes

In this subsection we determine the visibility and oscillation frequency of the Ramsey fringes in the remnant Bose-Einstein condensate and provide quantitative corroboration of the more physical arguments provided in Subsection II B. We shall provide the main physical ideas of the derivations in terms of the dynamics of a single pair of atoms and present the results of a genuine many-body treatment to clearly separate two-body phenomena from those specifically related to the coherent nature of the partially Bose condensed gas. The detailed derivations on the basis of the many-body approach are given in Appendix A. We restrict our analysis in this section to the ideal limit of Ramsey interferometry, in which the gas is weakly interacting during the evolution period.

1. *Atom-molecule interference of a single pair of atoms*

Motivated by the approaches of Refs. [32, 33], we first consider a pair of ^{85}Rb atoms in a spherically symmetric trap, exposed to a spatially homogeneous magnetic field, whose strength is varied in time, according to the sequence of pulses in Fig. 1. The degrees of freedom of the centre of mass and relative motions of the atom pair are then exactly decoupled, and the dynamics of the relative coordinate $\mathbf{r}$ is determined by a Hamiltonian of the form:

$$H_{2\mathrm{B}} = -\frac{\hbar^2}{m}\nabla^2 + V_{\mathrm{trap}}(r) + V(B, r). \tag{2}$$

Here $V_{\mathrm{trap}}(r)$ is the potential of the atom trap, m is the atomic mass, and $V(B, r)$ is the magnetic field dependent binary interaction potential. In general, $H_{2\mathrm{B}}$ depends on all hyperfine states of the atoms, which are strongly coupled by the Feshbach resonance state $\phi_{\mathrm{res}}(r)$ (cf., e.g., Refs. [20, 32] and Fig. 3). For simplicity, we shall suppress, throughout this paper, all indices related to the multichannel nature of the binary interactions. All our results and derivations are, however, quite general and can be applied to zero energy resonances with any number of relevant scattering channels.

The analogue of the condensate mode is realised by the lowest energetic state of two atoms above the dissociation threshold of the pair interaction potential $V(B, r)$, whose wave function $\phi_0(r)$ thus obeys the stationary Schrödinger equation $H_{2\mathrm{B}}\phi_0(r) = E_0\phi_0(r)$, with the two-body Hamiltonian evaluated at the initial magnetic field strength of the pulse sequence. The amplitude for the probability to detect the atoms in the state ϕ_0 at the final time t_{final} of the pulse sequence thus provides the analogue of the amplitude for the remnant condensate fraction, and is determined by:

$$T_{2B}(\phi_0 \leftarrow \phi_0) = \langle \phi_0 | U_{2B}(t_{\text{final}}, t_0) | \phi_0 \rangle. \tag{3}$$

Here $U_{2B}(t_{\text{final}}, t_0)$ is the time evolution operator, which satisfies the Schrödinger equation

$$i\hbar \frac{\partial}{\partial t} U_{2B}(t, t_0) = H_{2B}(t) U_{2B}(t, t_0). \tag{4}$$

Separating the pulse sequence in Fig. 1 into its different components, $U_{2B}(t_{\text{final}}, t_0)$ can be factorised into the evolution operators $U_{\#1}(t_1, t_0)$, $U_{\#2}(t_{\text{final}}, t_2)$ and $U_{\text{evolve}}(t_{\text{evolve}})$, associated with the first and second magnetic field pulse and with the evolution period of the sequence, respectively. Here t_1 is the time immediately after the first magnetic field pulse, t_2 is the time at the beginning of the second magnetic field pulse, and $t_2 - t_1 = t_{\text{evolve}}$ is the duration of the evolution period. The factorisation of $U_{2B}(t_{\text{final}}, t_0)$ yields:

$$U_{2B}(t_{\text{final}}, t_0) = U_{\#2}(t_{\text{final}}, t_2) U_{\text{evolve}}(t_{\text{evolve}}) U_{\#1}(t_1, t_0). \tag{5}$$

During the evolution period the magnetic field strength is constant and $U_{\text{evolve}}(t_{\text{evolve}})$ depends only on the duration t_{evolve}. It can therefore be written in terms of the stationary energy states of H_{2B} at the magnetic field strength B_{evolve} (cf. Fig. 1). This leads to the spectral decomposition:

$$U_{\text{evolve}}(t_{\text{evolve}}) = \sum_{v=-1}^{\infty} |\phi_v^{\text{evolve}}\rangle e^{-iE_v^{\text{evolve}} t_{\text{evolve}}/\hbar} \langle \phi_v^{\text{evolve}}|. \tag{6}$$

Here we have labelled the two-body energy states $\phi_v^{\text{evolve}}(r)$ by their vibrational quantum numbers, starting from the highest excited vibrational molecular bound state $\phi_{-1}^{\text{evolve}}(r) = \phi_{\text{b}}^{\text{evolve}}(r)$, whose energy $E_{\text{b}}(B_{\text{evolve}}) = E_{\text{b}}^{\text{evolve}}$ is depicted in Fig. 3, to the quasi continuum of excited states $\phi_v^{\text{evolve}}(r)$ ($v = 0, 1, 2, \ldots$) with energies above the dissociation threshold of $V(B_{\text{evolve}}, r)$. As the initial state, as well as the trap potential, are spherically symmetric, we have left out all energy states corresponding to partial waves with an orbital angular momentum different from $l = 0$. We have also neglected all vibrational molecular bound states with energies below $E_{\text{b}}(B_{\text{evolve}})$ because these states are energetically inaccessible.

Inserting Eq. (6) into Eq. (5), the transition amplitude in Eq. (3) can be represented in terms of a diffusion contribution $D_{2B}(t_{\text{evolve}})$, which is slowly varying in t_{evolve} and stems from the quasi continuum states, along with a comparatively rapidly varying oscillatory amplitude $A_{2B}(t_{\text{evolve}})$ associated with the spectral component of the molecular bound state:

$$T_{2B}(\phi_0 \leftarrow \phi_0) = D_{2B}(t_{\text{evolve}}) + A_{2B}(t_{\text{evolve}}). \tag{7}$$

Both amplitudes can be expressed in terms of the amplitudes

$$T_{2B}^{\#1}(\phi_v^{\text{evolve}} \leftarrow \phi_0) = \langle \phi_v^{\text{evolve}} | U_{\#1}(t_1, t_0) | \phi_0 \rangle, \tag{8}$$
$$T_{2B}^{\#2}(\phi_0 \leftarrow \phi_v^{\text{evolve}}) = \langle \phi_0 | U_{\#2}(t_{\text{final}}, t_2) | \phi_v^{\text{evolve}} \rangle \tag{9}$$

associated with the probabilities for transitions between $\phi_0(r)$ and the vibrational states $\phi_v^{\text{evolve}}(r)$ at the magnetic field strength B_{evolve} during the first and second magnetic field pulse. This gives the diffusion part to be

$$D_{2B}(t_{\text{evolve}}) = \sum_{v=0}^{\infty} T_{2B}^{\#2}(\phi_0 \leftarrow \phi_v^{\text{evolve}}) e^{-iE_v^{\text{evolve}} t_{\text{evolve}}/\hbar} \times T_{2B}^{\#1}(\phi_v^{\text{evolve}} \leftarrow \phi_0), \tag{10}$$

while the oscillatory amplitude is given by

$$A_{2B}(t_{\text{evolve}}) = T_{2B}^{\#2}(\phi_0 \leftarrow \phi_{\text{b}}^{\text{evolve}}) e^{-iE_{\text{b}}^{\text{evolve}} t_{\text{evolve}}/\hbar} \times T_{2B}^{\#1}(\phi_{\text{b}}^{\text{evolve}} \leftarrow \phi_0). \tag{11}$$

The probability $P_{0,0}(t_{\text{evolve}}) = |T_{2B}(\phi_0 \leftarrow \phi_0)|^2$ for the two atoms to be detected in the state $\phi_0(r)$ at the final time of the pulse sequence provides the two-body analogue of the remnant condensate fraction as a function of t_{evolve}. Neglecting the weak dependence of the diffusion term $D_{2B}(t_{\text{evolve}})$ on t_{evolve}, $P_{0,0}(t_{\text{evolve}})$ takes the well known form of an interference signal:

$$P_{0,0}(t_{\text{evolve}}) = |D_{2B}|^2 + |A_{2B}|^2 + 2\,|D_{2B}|\, \sqrt{P_{0,\text{b}}^{\#1} P_{\text{b},0}^{\#2}} \sin(\omega_{\text{e}} t_{\text{evolve}} + \Delta\varphi). \tag{12}$$

Here

$$P_{0,\text{b}}^{\#1} = \left| T_{2B}^{\#1}(\phi_{\text{b}}^{\text{evolve}} \leftarrow \phi_0) \right|^2, \tag{13}$$
$$P_{\text{b},0}^{\#2} = \left| T_{2B}^{\#2}(\phi_0 \leftarrow \phi_{\text{b}}^{\text{evolve}}) \right|^2 \tag{14}$$

are the probabilities for molecular formation and dissociation during the first and second magnetic field pulse, respectively, and

$$\omega_{\text{e}} = \left| E_{\text{b}}^{\text{evolve}} \right| / \hbar \tag{15}$$

is the angular frequency of the fringes. The total phase shift $\Delta\varphi$ involves the phases of the complex amplitudes in Eqs. (8) and (9), and of D_{2B}.

The signal in Eq. (12) has maxima and minima at the evolution times $t_{\text{evolve}}^{\max}$ and $t_{\text{evolve}}^{\min}$, which fulfil the relations

$$\sin\left(\omega_{\text{e}} t_{\text{evolve}}^{\max} + \Delta\varphi\right) = 1, \tag{16}$$
$$\sin\left(\omega_{\text{e}} t_{\text{evolve}}^{\min} + \Delta\varphi\right) = -1, \tag{17}$$

respectively. The visibility V_{Ramsey} of the Ramsey fringes produced by a single pair of atoms is thus given by:

$$V_{\text{Ramsey}} = \frac{P_{0,0}(t_{\text{evolve}}^{\max}) - P_{0,0}(t_{\text{evolve}}^{\min})}{P_{0,0}(t_{\text{evolve}}^{\max}) + P_{0,0}(t_{\text{evolve}}^{\min})} = 2\sqrt{P_{0,\text{b}}^{\#1} P_{\text{b},0}^{\#2} / P_{0,0}^{\text{avg}}}. \tag{18}$$

Here $P_{0,0}^{\text{avg}} = |D_{2B}|^2 + |A_{2B}|^2$ is the average signal obtained for evolution times t_{evolve}, at which the oscillatory part on the right hand side of Eq. (12) vanishes.

These derivations based on two-body physics reveal that the emergence of the Ramsey fringes in Refs. [7, 8] does not crucially rely upon the presence of many atoms in a Bose-Einstein condensate. The same kind of interferometry could be realised, for instance, also with two atoms in a tight atom trap of an optical lattice site. These atoms could be bosons or non-identical fermions, which both can interact with each other via s waves. The visibility of the fringe pattern is determined by the probability $P_{0,\mathrm{b}}^{\#1}$ of molecular production in the first magnetic field pulse and by the probability $P_{\mathrm{b},0}^{\#2}$ of their reconversion into atom pairs in the lowest energetic quasi continuum state $\phi_0(r)$, during the second magnetic field pulse. The angular frequency of the Ramsey fringes is solely determined by the binding energy $E_{\mathrm{b}}^{\mathrm{evolve}}$.

2. Continuum limit

To extend the two-body considerations to an effective description of a homogeneous gas of atoms, we shall first describe the limiting process as we move from the discrete trap states to a continuum. We thus assume that the two atoms are confined to a large volume $\mathcal{V}$, whose length scales greatly exceed the range of the inter-atomic forces as well as the spatial extent of the bound molecular state $\phi_{\mathrm{b}}^{\mathrm{evolve}}$. The products $\mathcal{V}P_{0,\mathrm{b}}^{\#1}$ and $\mathcal{V}P_{\mathrm{b},0}^{\#2}$ are then virtually independent of $\mathcal{V}$, and the coupling between the centre of mass and the relative coordinates of the atom pair is negligible. In the continuum limit, the amplitudes $T_{2\mathrm{B}}^{\#1}(\phi_{\mathrm{b}}^{\mathrm{evolve}} \leftarrow \phi_0)$ and $T_{2\mathrm{B}}^{\#2}(\phi_0 \leftarrow \phi_{\mathrm{b}}^{\mathrm{evolve}})$ contain the two-body time evolution operator and the bound molecular state $\phi_{\mathrm{b}}^{\mathrm{evolve}}$ in free space, as well as the limit of the lowest energetic quasi continuum state $|\phi_0\rangle$ to a zero momentum plane wave $|0\rangle$ of the relative motion of the atoms. This implies the formal replacement:

$$|\phi_0\rangle \to |0\rangle\sqrt{\frac{(2\pi\hbar)^3}{\mathcal{V}}}\,. \tag{19}$$

This choice of the initial state properly reflects the coherence properties of a Bose-Einstein condensate [34].

In contrast to molecular production or dissociation, the transfer between quasi continuum states involves a spatial range on the order of magnitude of the complete sample volume $\mathcal{V}$. This prevents us from performing the continuum limit directly in the elastic amplitude $T_{2\mathrm{B}}(\phi_0 \leftarrow \phi_0)$ of Eq. (3). We consider instead the continuum limit of the function

$$\begin{aligned} h(t,t_0) &= \mathcal{V} i\hbar\frac{\partial}{\partial t}\langle\phi_0|U_{2\mathrm{B}}(t,t_0)|\phi_0\rangle \\ &\to (2\pi\hbar)^3\langle 0|V(B(t))U_{2\mathrm{B}}(t,t_0)|0\rangle\theta(t-t_0), \end{aligned} \tag{20}$$

which is related to the elastic transition amplitude through the following:

$$T_{2\mathrm{B}}(\phi_0 \leftarrow \phi_0) = 1 - \frac{i}{\hbar\mathcal{V}}\int_{t_0}^{t_{\mathrm{final}}} dt\, h(t,t_0). \tag{21}$$

Here $\theta(t-t_0)$ denotes the step function, which yields unity for $t > t_0$ and zero elsewhere. The first term on the right hand side of Eq. (21) can to some extent be interpreted as the part of the amplitude associated with the events in which both atoms do not scatter, while the second term, proportional to the inverse of the volume, accounts for all possible collision events during the pulse sequence.

3. Probabilistic extension of the description of a single pair of atoms to the description of a homogeneous gas

A dilute gas usually occupies a volume $\mathcal{V}$ much larger than the volume needed for a single pair of atoms to collide and then separate to a distance outside the range of their binary interaction. The volume of the gas can thus be divided into regions that are small enough to contain at most two atoms but still sufficiently large to exceed the range of the inter-atomic forces by a large amount. This coarse graining procedure provides the physical justification for rescaling two-body transition amplitudes in order to describe a homogeneous gas of atoms with a density n. The correct scaling factor between the effective volume of two colliding atoms and the entire volume $\mathcal{V}$ of the gas can be determined from classical probability theory. When applied to the molecular conversion efficiency of the first magnetic field pulse, for instance, classical probability theory predicts the number $2N_{\mathrm{b}}^{\#1}$ of atoms, associated to molecules, relative to the total number $N = n\mathcal{V}$ of atoms in the gas to be:

$$\begin{aligned} 2\frac{N_{\mathrm{b}}^{\#1}}{N} &= \frac{2}{N}\,\frac{N(N-1)}{2}\,\frac{(2\pi\hbar)^3}{\mathcal{V}}\,|\langle\phi_{\mathrm{b}}|U_{\#1}(t_1,t_0)|0\rangle|^2 \\ &= n\mathcal{V}P_{0,\mathrm{b}}^{\#1}. \end{aligned} \tag{22}$$

Here $2/N$ is the number of atomic constituents of a single diatomic molecule relative to the total number of atoms, $N(N-1)/2 \approx N^2/2$ is the number of pairs of atoms in the gas, and the remaining factor $(2\pi\hbar)^3\,|\langle\phi_{\mathrm{b}}|U_{\#1}(t_1,t_0)|0\rangle|^2\,/\mathcal{V}$ is the probability for the association of a single pair of atoms in the continuum limit. The probabilistic extension of the description of a single pair of atoms to the description of a homogeneous gas thus consists in identifying the effective volume of a colliding pair of atoms by the inverse of the atomic density. This identification is quite intuitive, as $1/n$ is exactly the volume, in which, on average, a single atom can be found in a homogeneous gas. We thus replace the two-body amplitude on the right hand sides of Eq. (21) by

$$T_{2\mathrm{B}}^{\mathrm{gas}}(\phi_0 \leftarrow \phi_0) = 1 - n\frac{i}{\hbar}\int_{t_0}^{t_{\mathrm{final}}} dt\, h(t,t_0). \tag{23}$$

The probabilistic approach implies, in particular, that we should multiply the transition probabilities for molecular production or dissociation in Eqs. (13) and (14) by the number of atoms $N = n\mathcal{V}$. A similar procedure was previously applied by Mies *et al.* (cf. Refs. [20, 32]), leading to a remarkable agreement between theory and the Feshbach resonance crossing experiments of Ref. [35]. From its derivation given in this paper, however, it becomes apparent that the probabilistic extension of the two-body physics to the description of a gas is not restricted to Bose-Einstein condensates but could be applied also to the interacting pairs of atoms in dilute two component Fermi gases, boson-fermion mixtures or non-condensed Bose gases. A comparison between Eq. (23) and the dynamic equation (28) for the atomic mean field of the genuine many-body theory of Refs. [9, 10] implies that the applicability of the probabilistic extension of the two-body physics is restricted to time scales $t_{\text{final}} - t_0 \ll m/[2\hbar a(B_{\text{evolve}})n_c^{\text{evolve}}]$, where n_c^{evolve} is the mean condensate density during the evolution period, and $2\pi\hbar/\mu_{\text{evolve}} = m/[2\hbar a(B_{\text{evolve}})n_c^{\text{evolve}}]$ is the oscillation period associated with the chemical potential.

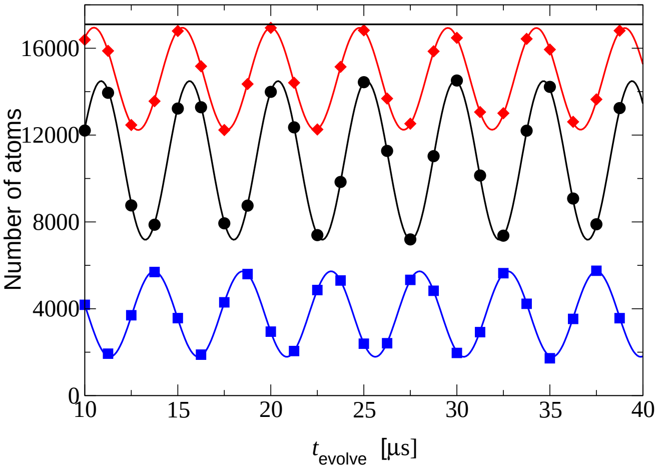

FIG. 4: Number of remnant condensate and burst atoms in dependence on t_{evolve}, as determined from the probabilistic extension of the two-body dynamics, evaluated at the mean experimental density [7] of 3.16×10^{12} cm^{-3}. All the other physical parameters and symbols are the same as those in Fig. 2.

Figure 4 shows the interference fringes predicted by the probabilistic extension of the two-body dynamics for the experimental situation described in Fig. 6 of Ref. [7]. The comparison between Fig. 2 of this paper and Fig. 6 of Ref. [7] on one hand and Fig. 4 on the other hand reveals that the two-body approach overestimates molecular production efficiencies and the fringe visibilities in a Bose-Einstein condensate. The overall qualitative features, as well as the order of magnitude of all components, however, correctly reflect the predictions of full many-body simulations as well as the experimental observations. The predictive power of such a simple approach based on classical probability theory is even more remarkable in view of the fact that the widely used two level mean field approach of Refs. [12, 13, 14, 15, 16, 17, 18] fails completely to describe the fringe pattern. In fact, this version of a many-body mean field theory not only rules out the production of burst atoms [20] but it also predicts, when applied to the physical situation of Fig. 6 in Ref. [7], that the number of condensate atoms should remain virtually unchanged, throughout the entire pulse sequence. This failure of the two level mean field approach is due to its incomplete description of the binary collision physics [20].

Equation (18) implies that the visibility of the interference fringes in the remnant Bose-Einstein condensate is given by

$$V_{\text{Ramsey}} = 2n\mathcal{V}\sqrt{P^{\#1}_{0,\text{b}}P^{\#2}_{\text{b},0}/P^{\text{avg}}_{0,0}}, \qquad (24)$$

where $P^{\text{avg}}_{0,0}$ can be obtained from the transition amplitude in Eq. (23) and thus converges to unity in the limit of zero density. The product $\mathcal{V}\sqrt{P^{\#1}_{0,\text{b}}P^{\#2}_{\text{b},0}}$ is independent of the density n and of the volume $\mathcal{V}$. Consequently, the visibility V_{Ramsey} varies linearly with the density in the limit $n \to 0$. The probabilistic approach recovers the angular frequency of the Ramsey fringes of the associated two-body problem in Eq. (15).

4. *Molecular production efficiency*

The visibility of the Ramsey fringes in Eq. (24) strongly depends on the molecular production efficiency $P^{\#1}_{0,\text{b}}$, during the first magnetic field pulse of the sequence in Fig. 1. In the course of the molecular association, pairs of atoms separated by the average inter-atomic distance of the gas are transferred into a highly excited but comparatively tightly bound state, with a mean internuclear distance on the order of $\langle r \rangle = a(B_{\text{evolve}})/2$. These length scales typically differ by several orders of magnitude, and special techniques are required to efficiently overcome the problem of the large spatial separation of atoms in a dilute gas.

The technique of magnetic field pulses, applied in Refs. [7, 8], uses two steps to achieve molecular association. First, the magnetic field strength is swept close to the zero energy resonance, so that the scattering length $a(B_{\text{min}})$ becomes comparable in magnitude to the mean inter-atomic distance of the gas. From the intermediate length scale set by $a(B_{\text{min}})$ the atom pairs are then transferred to their mean internuclear distance of $\langle r \rangle = a(B_{\text{evolve}})/2$ in the final upward ramp of the first magnetic field pulse. This physical picture suggests that an efficient molecular association requires a favourable balance between the mean inter-atomic distance of the gas and the scattering lengths $a(B_{\text{min}})$ and $a(B_{\text{evolve}})$. A similar balance of length scales is also required to achieve favourable Franck-Condon overlaps between initial and final molecular states in the general context of molecular spectroscopy [36]. Our analytic studies of Appendix B, indeed, indicate that the mechanism of molecular production with magnetic field pulses exhibits analogies to the experimental technique of two colour photo-association (see Ref. [37] for a description of the technique), in which free pairs of atoms are transferred into a comparatively tightly bound molecule via Raman transitions through a highly excited intermediate state. While the photo-association approach can populate a single deeply bound target level, by appropriately tuning the laser frequencies, the molecular production via magnetic field pulses involves a range of energies that overlap with the continuum part of the two-body spectrum. This reduces the efficiency of the association of molecules in the highest excited diatomic vibrational bound state and leads to the observed production of burst atoms [7].

These considerations are confirmed by the results on the molecular production efficiency in the first pulse of the mag-

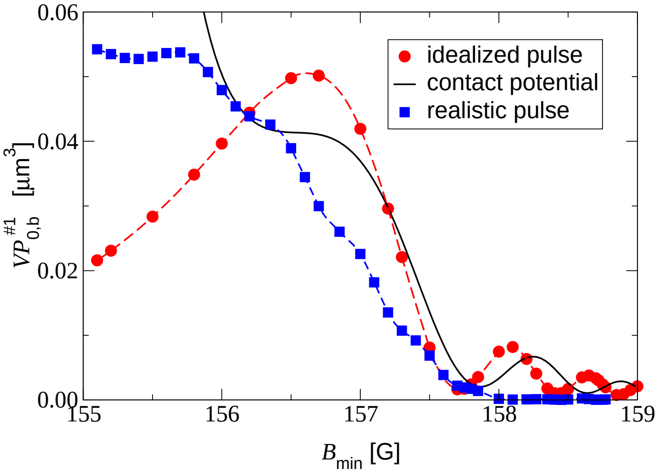

FIG. 5: The molecular production efficiency $P^{\#1}_{0,\mathrm{b}}$ as a function of the minimum magnetic field strength B_{min}, during the first pulse of the sequence of Fig. 1, for a fixed evolution field strength of $B_{\mathrm{evolve}} = 160$ G. The figure compares molecular production efficiencies of the realistic pulse of Fig. 1 (squares) with predictions associated with an idealised pulse sequence (cf. Appendix A), which just contains sudden changes of the magnetic field strength. These predictions involve calculations using a realistic low energy binary interaction potential [10, 19, 20] (circles and squares) and the contact potential approximation of Appendix B (solid curve). The duration of the idealised first magnetic field pulse of the sequence was chosen to be 36.2 μs.

netic field sequence presented in Fig. 5. For the case of an idealised pulse sequence, consisting of sudden jumps of the magnetic field strength, we observe an optimal value of B_{min} of around 156.7 G, where a favourable balance between the three inter-particle length scales involved in this process is reached. The analogous calculation performed for the realistic pulse sequence determines the optimal value of B_{min} to be smaller than 155.7 G, in agreement with the pulse sequence actually employed in the experiments of Refs. [7, 8]. Although both the realistic and idealised pulse sequence calculations predict the same order of magnitude for the molecular production efficiency, they significantly differ in their precise dependences on the magnetic field B_{min}. This reveals the sensitivity of the molecular component produced, and, as a consequence, of the observed fringe visibility, to the precise shape of the magnetic field pulse used. Figure 5 also shows that the analytic estimate of the molecular production efficiency in the contact potential approximation for the idealised pulse sequence (see Appendix B for details) recovers both the magnitude and the essential features of the predictions based on a realistic low energy binary interaction potential. For the values of B_{min} smaller than 156 G we are outside the domain of the analytical approximation, as explained in Appendix B. For the idealised pulse sequence we observe effects of quantum interference in the inelastic transition amplitude resulting in the oscillations of the transition probability for B_{min} greater than 157 G. These interference phenomena in inelastic transition amplitudes are sometimes referred to as Stückelberg oscillations [38] (see, e.g., Ref. [39] for similar interferences in three-body recombination rate constants).

5. *Many-body corrections to the frequency and visibility of the Ramsey fringes in the remnant Bose-Einstein condensate*

The main differences between the effective two-body and the genuine many-body descriptions of dilute Bose-Einstein condensates reside in the treatment of the coherent nature of the gas and of the non-linear dynamics of the atomic mean field. In Appendix A we provide a detailed derivation of the many-body corrections to the frequency and visibility of the Ramsey fringes in the remnant Bose-Einstein condensate, under the assumption that the gas is weakly interacting during the evolution period of the pulse sequence. In this section we give a physical explanation of their origin. For simplicity, we shall consider all quantities in the homogeneous gas limit.

The coherent dynamics of the atomic mean field $\Psi(t)$, during the evolution period, is largely described by the stationary limit $\Psi(t) \propto (n_{\mathrm{c}}^{\mathrm{evolve}})^{1/2} \exp(-i\mu_{\mathrm{evolve}} t/\hbar)$, up to a global phase shift, where $n_{\mathrm{c}}^{\mathrm{evolve}}$ is the mean condensate density and

$$\mu_{\mathrm{evolve}} = 4\pi\hbar^2 a(B_{\mathrm{evolve}}) n_{\mathrm{c}}^{\mathrm{evolve}}/m \tag{25}$$

is the chemical potential. The chemical potential can thus be largely interpreted as the amount of energy gained by each atom due to the presence of the surrounding atoms. We thus expect that the finite energy of $2\mu_{\mathrm{evolve}}$ in a binary collision leads to an upward shift of the two-body angular fringe frequency in Eq. (15), which yields:

$$\omega_{\mathrm{e}} = \left(\left|E_{\mathrm{b}}^{\mathrm{evolve}}\right| + 2\mu_{\mathrm{evolve}}\right)/\hbar. \tag{26}$$

This is precisely the estimate that we obtain from the systematic treatment given in Appendix A.

We note, however, that the Gross-Pitaevskii approximation of the chemical potential in Eq. (25) becomes singular when the magnetic field strength approaches the zero energy resonance. This singularity is an artifact of the assumption of weak interactions, i.e. $n_{\mathrm{c}}^{\mathrm{evolve}} a^3(B_{\mathrm{evolve}}) \ll 1$, during the evolution period. The Gross-Pitaevskii approximation of Eq. (25) may be systematically improved using the self consistent treatment of Ref. [19], which determines the chemical potential in terms of the exact stationary solution of the genuine many-body dynamic equation (28) for the atomic mean field [40]. This stationary approach leads to a chemical potential, which properly accounts for the energy dependence of the binary transition amplitudes [19] and leads to the physically expected smooth behaviour of μ_{evolve} when the magnetic field strength is tuned in the close vicinity of the zero energy resonance.

Our studies of Section III also indicate that even in the absence of deeply inelastic loss processes, like, e.g., spin relaxation, the experimental [7, 8] evolution times t_{evolve} are too short for the gas to equilibrate. In particular, t_{evolve} is typically much smaller than the time scale $\hbar/(2\mu_{\mathrm{evolve}})$ set by the many-body frequency shift in Eq. (26). As a consequence, the experiments [7, 8] could not fully resolve the frequency shift.

The derivations in Appendix A reveal that the many-body corrections to the visibility in Eq. (24) are mainly due to the non-linear dynamics of the atomic mean field. The final result

$$V_{\text{Ramsey}} = \frac{1 - \exp\left(-4n\mathcal{V}\left[P^{\#1}_{0,\text{b}}P^{\#2}_{\text{b},0}\right]^{1/2}\right)}{1 + \exp\left(-4n\mathcal{V}\left[P^{\#1}_{0,\text{b}}P^{\#2}_{\text{b},0}\right]^{1/2}\right)} \qquad (27)$$

largely recovers the dependences of Eq. (24) on the physical parameters n, $\mathcal{V}P^{\#1}_{0,\text{b}}$ and $\mathcal{V}P^{\#2}_{\text{b},0}$, so that both formulae asymptotically coincide in the limit $n \to 0$. The non-linear nature of the mean field dynamics, however, leads to a reduction of the fringe visibility in comparison with the probabilistic extension of the linear two-body time evolution, when the density is increased. A similar behaviour can be observed in the comparison between genuine many-body predictions and the extended two-body Landau-Zener approach of Ref. [32] for the description of the molecular production in Feshbach resonance crossing experiments with linear ramps of the magnetic field strength [20].

III. DECOHERENCE OF THE RAMSEY FRINGES

In this section we consider in detail the regime of magnetic field strengths in the close vicinity of the zero energy resonance, in which decoherence phenomena diminish the Ramsey fringes in the remnant Bose-Einstein condensate. This regime of low molecular vibrational frequencies is strongly influenced by the non-linear dynamics of the atomic mean field. Our numerical simulations are therefore based on the many-body approach of Refs. [9, 10] that includes both a non-perturbative treatment of the binary physics and the nonlinearities to all orders in the atomic mean field.

A. Comparison between experimental Ramsey fringes in the remnant Bose-Einstein condensate and many-body simulations

In the first order microscopic quantum dynamics approach of Refs. [9, 10] the evolution of all components of the gas is determined by a single non-linear Schrödinger equation for the atomic mean field, i.e.

$$i\hbar\frac{\partial}{\partial t}\Psi(\mathbf{x},t) = \left[-\frac{\hbar^2}{2m}\nabla^2 + V_{\text{trap}}(\mathbf{x})\right]\Psi(\mathbf{x},t) - \Psi^*(\mathbf{x},t)\int_{t_0}^{\infty} d\tau\, \Psi^2(\mathbf{x},\tau)\frac{\partial}{\partial\tau}h(t,\tau). \qquad (28)$$

The inter-atomic collisions are included fully in this approach in the time dependent coupling function of Eq. (20). The dynamics of the atomic mean field determines not only the condensate density $n_c(\mathbf{x},t) = |\Psi(\mathbf{x},t)|^2$ but also the molecular and burst fractions of the gas [10]. The simulations of the final number of atoms of all components of the gas in Fig. 2 correspond to the experimental situation of Fig. 6 in Ref. [7], and were obtained from a sequence of full solutions of Eq. (28) with variable evolution times.

In the course of our studies, we have solved Eq. (28) for a variety of experimental [8] evolution times t_{evolve} and magnetic field strengths B_{evolve}. Our simulations fully account for realistic sequences of magnetic field pulses [25], shown schematically in Fig. 1, and for the inhomogeneous nature of the Bose-Einstein condensate in a cylindrical atom trap with the experimental radial and axial frequencies of $\nu_{\text{radial}} = 17.5$ Hz and $\nu_{\text{axial}} = 6.8$ Hz, respectively. The initial state of our simulations is the ground state of the stationary Gross-Pitaevskii equation, corresponding to a ^{85}Rb Bose-Einstein condensate with 16000 atoms [8] at the initial magnetic field strength of $B = 162.2$ G of the pulse sequence in Fig. 1.

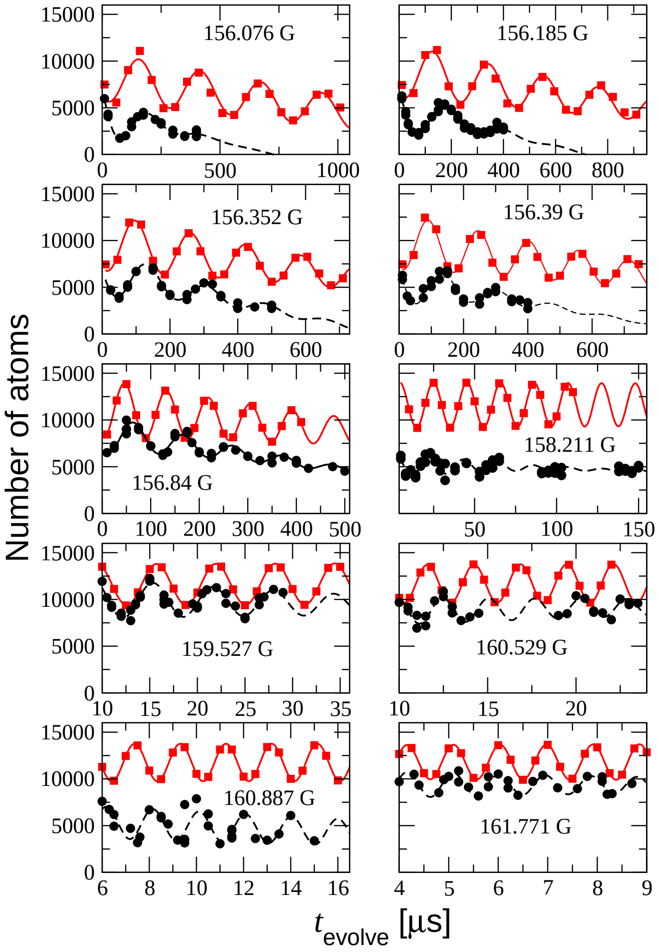

FIG. 6: Comparison of the experimental [8, 25] number of atoms in the remnant Bose -Einstein condensate as a function of t_{evolve} (circles) with the predictions of Eq. (28) (squares) at the end of each magnetic field pulse sequence. The dashed and solid curves indicate the fits of Eq. (29) [8] to the experimental and theoretical data, respectively. In the course of the experiments [8], the magnetic field strength B_{evolve} during the evolution period of the pulse sequence was varied between 156.076 and 161.771 G. The fringe patterns cover a wide range of evolution times, from about 10 μs at 161.771 G to about 1 ms at 156.076 G.

Figure 6 shows comparisons between the experimentally observed dependence on t_{evolve} of the remnant condensate and theoretical predictions of Eq. (28), at the end of each magnetic field pulse sequence. Both the experimental data and the theoretical predictions exhibit damped oscillations, whose decay becomes particularly marked for sequences with longer evolution times on the order of 1 ms, at magnetic field strengths of $B_{\mathrm{evolve}} \lesssim 157$ G, i.e. in the close vicinity of the zero energy resonance at $B_0 = 155.041$ G [8]. The theoretical predictions have the same systematic trends as the experimental fringe patterns with frequencies between 4 kHz at 156.076 G and about 1 MHz at 161.771 G. All of the theoretical curves overestimate the measured numbers of remnant condensate atoms. These deviations may, at least in principle, be due to fast inelastic loss phenomena such as spin relaxation in ^{85}Rb collisions, whose rates are enhanced in the vicinity of the zero energy resonance [24]. We shall show in Subsection III C, however, that spin relaxation is unlikely to play a dominant role in these deviations. Our results of Subsection II C rather indicate that the remnant condensate fractions in the interferometric experiments are very sensitive to the precise shape of the magnetic field pulse sequence. We therefore believe that a mismatch between the real experimental pulse sequence and the sequence used in our simulations is a more likely reason for the deviations, in particular, for magnetic field strengths $B_{\mathrm{evolve}} \gtrsim 158$ G, away from the position of the zero energy resonance.

B. Oscillation frequencies of the Ramsey fringes in the remnant Bose-Einstein condensate

In order to extract the fringe frequencies from our simulations, we have closely followed the procedure suggested in Ref. [8] and fitted the theoretically predicted dependence of the number of remnant condensate atoms on t_{evolve} to the formula:

$$N_{\mathrm{c}}^{\mathrm{evolve}} = N_{\mathrm{avg}} - \alpha t_{\mathrm{evolve}} + A e^{-\beta t_{\mathrm{evolve}}} \sin\left(\omega_{\mathrm{e}} t_{\mathrm{evolve}} + \Delta\varphi\right). \tag{29}$$

The angular frequency ω_{e} of the fringes has been interpreted in Ref. [8] in terms of a natural oscillation frequency ν_0, which is related to the angular frequency ω_{e} through $\omega_{\mathrm{e}} = 2\pi\sqrt{\nu_0^2 - [\beta/(2\pi)]^2}$. The amplitude A of the interference fringes as well as the average number N_{avg} of atoms determine the fringe visibility. The remaining fit parameters are a loss rate of atoms α, a damping rate β and a phase shift $\Delta\varphi$ of the Ramsey fringes. We note that the fit parameters of Eq. (29) can be largely identified from the interference signal of a single pair of atoms in Eq. (12), provided that the weak dependence of the diffusion contribution $D_{2\mathrm{B}}(t_{\mathrm{evolve}})$ on the evolution time t_{evolve} is taken into account. The fit at $B_{\mathrm{evolve}} = 156.076$ G in Fig. 6 indicates, however, that the functional form of Eq. (29) is not entirely compatible with the non-linear dynamics of the atomic mean field in Eq. (28).

Figure 7 shows the natural frequency ν_0 in dependence on B_{evolve} as obtained from the fits to the experimental and theoretical data in Fig. 6, respectively. As pointed out in Refs. [7, 10, 26], for magnetic field strengths $B_{\mathrm{evolve}} > 158$ G, sufficiently far away from the zero energy resonance at $B_0 = 155.041$ G, the fringe frequencies closely match the vibrational frequencies associated with the weakly bound molecular state $\phi_{\mathrm{b}}^{\mathrm{evolve}}$. A comparison with Fig. 3 shows that the binding energies in this range of magnetic field strengths are sensitive to the long range van der Waals dispersion coefficient C_6 [10] and even to the magnetic moment dE_{res}/dB of the Feshbach resonance level (cf.,e.g., Refs. [20, 32]), which determines the linear slope of $E_{\mathrm{b}}(B)$ at magnetic field strengths $B_{\mathrm{evolve}} > 162$ G.

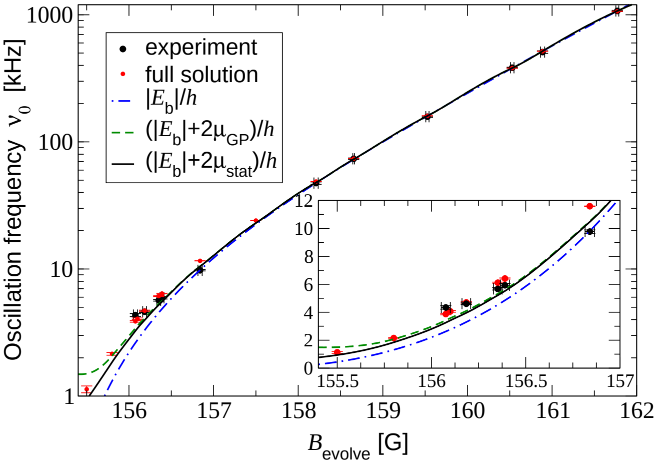

FIG. 7: Natural frequency ν_0 of the Ramsey fringes as a function of the magnetic field strength B_{evolve} as obtained through fits of the theoretical predictions (squares) and of the experimental [8, 25] number of remnant condensate atoms (circles) to Eq. (29). The solid and dashed curves indicate theoretical predictions of the fringe frequency that account for the first order many-body contribution $2\mu_{\mathrm{evolve}}/h$ (cf. Subsection II C) of the chemical potential in the self consistent stationary approach of Ref. [19] (solid curve) and in the Gross-Pitaevskii approximation of Eq. (25) (dashed curve), respectively. The dotted dashed curve shows the binding frequency of the highest excited vibrational molecular bound state of ^{85}Rb$_2$, in dependence on the magnetic field strength. The inset shows an enlargement of the near resonance region of magnetic field strengths B_{evolve}, in which the deviations between fringe frequency and molecular vibrational frequency become apparent. Small error bars in the theoretical data result from the uncertainties associated with the fitting procedure.

Closer to the zero energy resonance both the experimental data [8] as well as the theoretical predictions show a visible upward shift of the fringe frequencies from the molecular vibrational frequencies. From the analytic results of our theoretical studies in Section II and from our numerical simulations we expect this shift to persist for all values of B_{evolve} but to decrease in its relative magnitude with increasing magnetic field strengths. The four experimental points closest to the zero energy resonance, to which a shift has been attributed in the experimental reference [8], agree in their magnitudes with our theoretical predictions (see inset of Fig. 7). For magnetic field strengths $B_{\mathrm{evolve}} \geq 156.84$ G the shift was neglected in Ref. [8] and the associated fringe frequencies were used to adjust the theoretical curve of the binding frequencies in Figs. 3 and 7. This, in turn, also determines the parameters B_0, ΔB and a_{bg}

of Eq. (1). As we have used these parameters as an input to the coupling function $h(t,\tau)$ of Eq. (28), and the frequency shift persists for all magnetic field strengths B_{evolve} in our approach, we expect our simulations to deviate slightly from the experimental findings simply due to the slight uncertainty in the Feshbach resonance parameters.

C. Two-body decay of the Bose-Einstein condensate

Despite the fact that the fit parameter α of Eq. (29) is determined with a much larger uncertainty than the frequency ν_0, we may interpret it in terms of two-body decay processes during the evolution period. Two-body loss phenomena in a Bose-Einstein condensate are quite generally described by the rate equation

$$\dot{N}_{\mathrm{c}}(t) = -\frac{K_2}{2}\langle n_{\mathrm{c}}(t)\rangle N_{\mathrm{c}}(t). \tag{30}$$

Here K_2 is the two-body loss rate constant, $\langle n_{\mathrm{c}}(t)\rangle$ is the average condensate density, and $N_{\mathrm{c}}(t)$ is the number of condensate atoms. We note that Eq. (30) is not restricted to the description of spin relaxation events but refers to all two-body loss phenomena which occur on time scales much shorter than those set by the bulk motion of the gas. We shall restrict our considerations on the two-body decay to magnetic field strengths $B_{\mathrm{evolve}} < 157$ G in the close vicinity of the zero energy resonance, where we find that the pulse sequences are sufficiently long to provide reliable values for α with a systematic trend as a function of B_{evolve}. In this region the Ramsey fringes of Fig. 6 also exhibit a strong decoherence, and diatomic molecules in the highest excited vibrational bound state can not be identified as a separate entity because their wave functions would be more extended than the mean interatomic distance of the gas [11]. In order to establish the relationship between α and K_2, we solve Eq. (30) formally by dividing both sides by $N_{\mathrm{c}}(t)$ and then integrating the logarithmic derivative from the time t_1, immediately after the first magnetic field pulse of Fig. 1, to the time t_2, immediately after the evolution period. This yields:

$$N_{\mathrm{c}}(t_2) = N_{\mathrm{c}}(t_1)\exp\left(-\frac{K_2}{2}\int_{t_1}^{t_2} dt\,\langle n_{\mathrm{c}}(t)\rangle\right). \tag{31}$$

If we assume that during the evolution period $t_{\mathrm{evolve}} = t_2 - t_1$ the loss of condensate atoms is small in comparison with $N_{\mathrm{c}}(t_1)$, we can expand the right hand side of Eq. (31) to first order in t_{evolve}. This leads to the following expression:

$$N_{\mathrm{c}}(t_2) \approx N_{\mathrm{c}}(t_1) - \frac{K_2}{2}N_{\mathrm{c}}(t_1)\langle n_{\mathrm{c}}(t_1)\rangle t_{\mathrm{evolve}}. \tag{32}$$

A comparison between Eqs. (29) and (32) then allows us to identify the parameters $N_{\mathrm{c}}(t_1) = N_{\mathrm{avg}}$, $N_{\mathrm{c}}(t_2) = N_{\mathrm{c}}^{\mathrm{evolve}}$ and

$$K_2 = \frac{2\alpha}{N_{\mathrm{avg}}\langle n_{\mathrm{c}}(t_1)\rangle}, \tag{33}$$

provided that the second magnetic field pulse does not significantly change the number of condensate atoms. Our numerical simulations show that this assumption is justified for longer pulse sequences with evolution fields $B_{\mathrm{evolve}} < 157$ G (cf. Fig. 6), while for the faster sequences it may be violated.

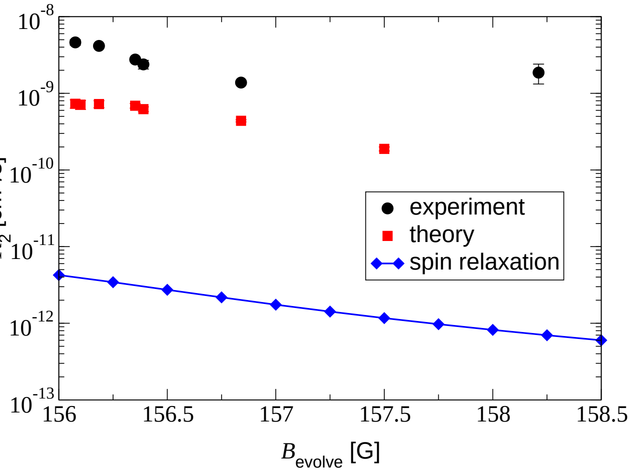

FIG. 8: The two-body loss rate constant K_2 determined from the fit parameter α of Eq. (29) through Eq. (33) as a function of the magnetic field strength B_{evolve} during the evolution period of the pulse sequence. The circles indicate the experimental values [8], while the squares correspond to the theoretical predictions of Eq. (28) depicted in Fig. 6. The error bars indicate the statistical errors of the fits. The solid curve indicates coupled channels calculations [41] of the spin relaxation rate constant for a pair of ^{85}Rb atoms in the limit of zero collision energy. The rate constant K_2 is given on a logarithmic scale.

Figure 8 provides an overview of the magnitudes of the two-body loss rate constants K_2 obtained through Eq. (33) from the fits to the experimental data [8] (circles) and to the theoretical predictions (squares) of Fig. 6. The rate constants K_2 are shown as a function of the magnetic field strength B_{evolve} during the evolution period. For comparison, the solid curve indicates results of a coupled channels calculation [41] of the spin relaxation rate constant. The comparatively large size of about 10^{-9} cm^3/s of both the experimental [8] and theoretical rate constants strongly indicate that the loss of condensate atoms is mainly due to the energy transfer from the first magnetic field pulse. This drives the initially weakly interacting Bose-Einstein condensate into a strongly correlated non-equilibrium state. Deeply inelastic spin relaxation loss phenomena are not included in our simulations of Eq. (28). The theory thus predicts that the atoms are transferred from the condensate into correlated pairs of atoms in excited states. The coupled channels calculations [41], indeed, confirm that the rate constants for spin relaxation (solid curve in Fig. 8) are less than 10^{-11} cm^3/s in the relevant range of magnetic field strengths, i.e. from 156 to 158.5 G, and thus do not explain the size of the observed losses. Our interpretation is corroborated by the observation of Ref. [8] that over the whole range of magnetic field strengths B_{evolve} the loss rate α is weakly dependent on B_{evolve} and consistent with the number loss in a single magnetic field pulse [42].

D. Visibility of the Ramsey fringes in the remnant Bose-Einstein condensate

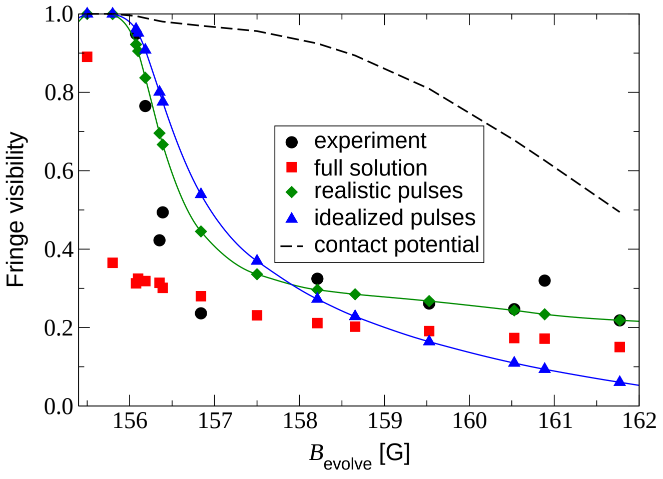

FIG. 9: Visibility of the Ramsey fringes in the remnant Bose-Einstein condensate determined from the experimental data (circles) and from the solutions of Eq. (28) (squares), as a function of the magnetic field strength B_{evolve} during the evolution period of the pulse sequence. We have also plotted the estimate of the fringe visibility given by Eq. (27), evaluated for the magnetic field pulses of the realistic sequence (diamonds) and of an idealised pulse sequence with sudden changes of the magnetic field strength (cf. Appendix A) (triangles). For the idealised pulse sequence the durations of the first pulse and the second pulse were chosen to be 36.2 μs and 23.9 μs, respectively. Equation (27) has then been evaluated for $n = 3.07 \times 10^{12}$ cm^{-3}, which corresponds to the initial mean density of the condensate in the experiments of Ref. [8]. The dashed curve shows the predictions of the contact potential approximation to the probabilities $P_{0,\text{b}}^{\#1}$ and $P_{\text{b},0}^{\#2}$ in Eq. (27).

Figure 9 shows the fringe visibility in the remnant Bose-Einstein condensate. This is determined as a function of the magnetic field strength B_{evolve} in the evolution period from the experimental data and from the full solutions of Eq. (28). The visibilities were obtained from the fits of Eq. (29) to the experimental and numerical data of Fig. 6 using the relation

$$V_{\text{Ramsey}} = A/N_{\text{avg}}. \tag{34}$$

The theoretical results follow the rough size and monotonic trend of the experimental visibilities. The increase of V_{Ramsey} with decreasing B_{evolve} is due to the enhanced depletion of the average number N_{avg} of remnant condensate atoms at magnetic field strengths close to the zero energy resonance. This trend can also be observed in the visibilities estimated from Eq. (27). These estimates were obtained from the exact transition probabilities $P_{0,\text{b}}^{\#1}$ and $P_{\text{b},0}^{\#2}$ for both the pulses of the realistic sequence (as depicted in Figure 1) and their counterparts in an idealised pulse sequence of sudden changes of the magnetic field strength (cf. Appendix A). Figure 9 also shows an estimate of V_{Ramsey} based on Eq. (27) and the contact potential approximation (cf. Appendix B). The contact potential approximation accounts for the inter-atomic interactions just in terms of a single parameter, the scattering length $a(B)$. The large difference between the contact potential approximation and the experimental data as well as the exact theoretical data reveals the sensitivity of the interferometric experiments of Refs. [7, 8] to the nature of inter-atomic interactions beyond universal considerations, which are based solely on the scattering length. This sensitivity of the Ramsey interferometry with atoms and molecules [7, 8] to non-universal properties of the binary collision physics provides a crucial probe of the microscopic physics through the bulk properties of the gas. The information it provides is largely inaccessible to experimental studies involving linear ramps of the magnetic field strength across zero energy resonances [19, 20].

IV. CONCLUSIONS

Our theoretical studies in this paper reveal the remarkable range of physical regimes that are probed by the atom-molecule coherence experiments of Refs. [7, 8]. These regimes include the Ramsey interferometer limit, at evolution fields sufficiently far away from the zero energy resonance for the binary and bulk motions to be virtually decoupled. In the other limit, i.e. the close vicinity of the zero energy resonance, two- and many-body phenomena can not be disentangled during the evolution period.

Using a probabilistic extension of the dynamics of a single pair of atoms to the description of a gas, we have clearly identified the different elements of a Ramsey interferometer from the experimental [7, 8] sequences of magnetic field pulses. We have shown that much of the observations of Refs. [7, 8], in particular, the frequency and visibility of the Ramsey fringes, can be understood qualitatively and also largely quantitatively on the basis of two-body physics. Our studies reveal that the probabilistic extension of the pair dynamics is applicable provided that the experiments are operated in the interferometer mode, i.e. at evolution fields far away from the zero energy resonance. These studies were motivated by the approaches of Refs. [32, 33]. Our probabilistic approach, however, is not restricted to Bose-Einstein condensates and does not include any adjustable parameters.

We have shown that in the interferometer mode, in contradiction to the interpretations of some previous theoretical studies [21, 26, 27], the gas is virtually unaffected by non-equilibrium phenomena during the evolution period of the pulse sequence, and the mutually orthogonal molecular and free atomic components evolve independently and coherently. The Ramsey fringes thus reflect the phase difference of both components rather than dynamical exchange of particles between them. In fact, such an exchange between the molecular and free atomic components during the evolution period would imply the breakup and reformation of molecules. In the absence of any external driving force these would be energetically impossible.

In the Ramsey interferometer mode the measurements provide detailed insight into the binary collision dynamics beyond universal considerations. These interferometric experiments are thus sensitive to the long range van der Waals dispersion coefficient C_6 of the binary interactions and even to the magnetic moment of the Feshbach resonance level, rather than just to the scattering length. Our studies clearly show that this sensitivity is observed not only in the fringe frequencies but also in their visibilities. The existence of the fringe pattern and its dependence on the physical parameters of the system is remarkable in its own right with the experiments clearly showing how vibration of molecules on a nanometre length scale can significantly influence the dynamics of the entire gas on length scales as large as several micrometres. This access to the microscopic physics can not easily be gained from the molecular association techniques based on linear ramps of the magnetic field strength across zero energy resonances, which are mainly sensitive just to universal scattering observables [19, 20].

Operated in the close vicinity of the zero energy resonance, the gas is driven into a strongly correlated non-equilibrium state during the evolution period. In this regime the binary collision physics and many-body phenomena can not be disentangled because the wave function of the highest excited diatomic vibrational bound state strongly overlaps with the mean distance between the atoms in the dilute gas [11]. A theoretical description of the observations of Ref. [8] thus requires genuine many-body considerations, which fully account not only for the two-body physics but also for the non-linear dynamics of the atomic Bose-Einstein condensate in a non-perturbative manner. Our dynamical simulations of all experiments of Ref. [8] were based on the microscopic quantum dynamics approach to dilute Bose-Einstein condensates of Refs. [9, 10] and explained all the systematic trends that we were able to identify from the measured data. These trends involve an upward frequency shift of the interference fringes, accompanied by decoherence and an overall decay of the condensate. We have shown that the degree to which these phenomena influence the fringe pattern can be interpreted as a measure of the extent to which molecules in the highest excited diatomic vibrational bound state can be identified as a separate entity of the gas. Our simulations indicate that even in the physical regime close to the zero energy resonance, in which the pulse sequences are sufficiently long to reveal a decay of the condensate, the non-equilibrium dynamics is determined mainly by the same physical parameters of the binary interaction potential as in the interferometer mode. Deeply inelastic loss processes, such as spin relaxation, are likely to be negligible. Such processes will, however, affect the parts of the experiment after the magnetic field pulse sequence, involving the ballistic expansion of the gas before imaging. On such longer time scales spin relaxation leads to the spontaneous dissociation of the molecules into fast fragments, which explains the presence of the component of undetected atoms [41, 43].

Acknowledgments

We are particularly grateful to Eleanor Hodby, Sarah Thompson and Carl Wieman for providing the experimental data to us, and to Servaas Kokkelmans for sharing with us the results of the coupled channels calculations of the binding energy of $^{85}\mathrm{Rb}_2$. We thank Thomas Gasenzer and Paul Julienne for interesting discussions. This research has been supported through a E.C. Marie Curie Fellowship under Contract no. HPMF-CT-2002-02000 (K.G.) and a University Research Fellowship of the Royal Society (T.K.). K.B. thanks the Royal Society and the Wolfson Foundation.

APPENDIX A: MANY-BODY DYNAMICS OF THE BOSE-EINSTEIN CONDENSATE

In this appendix we derive the formulae for the frequency and visibility of the Ramsey fringes in the remnant Bose-Einstein condensate [cf. Eqs. (26) and (27)] from the first order microscopic quantum dynamics approach of Refs. [9, 10]. We restrict our considerations to the region of magnetic field strengths B_{evolve}, in which the gas is weakly interacting during the evolution period of the pulse sequence. In this ideal limit of the Ramsey interferometry with atoms and molecules in a Bose-Einstein condensate the phenomena associated with the non-linear dynamics of the atomic mean field are weak. For simplicity, we perform all derivations in the homogeneous gas limit.

1. Hydrodynamic representation

In the homogeneous gas limit the atomic mean field $\Psi(t)$ depends just on the time variable t. To study the interference fringes, it is convenient to represent $\Psi(t)$ in terms of its uniform density and phase:

$$\Psi(t) = \sqrt{n_{\mathrm{c}}(t)}e^{-i\varphi(t)}. \tag{A1}$$

In this representation we then introduce the exponential form

$$n_{\mathrm{c}}(t) = e^{-2\gamma(t)} \tag{A2}$$

of the density. The evolution of the exponent $\gamma(t)$ as well as the phase $\varphi(t)$ are determined simultaneously by the real and imaginary parts of the dynamic equation for the atomic mean field, i.e. by

$$\dot{\gamma}(t) + i\dot{\varphi}(t) = -\frac{i}{\hbar}e^{2i\varphi(t)}\int_{t_0}^{\infty} d\tau\; e^{-2[\gamma(\tau)+i\varphi(\tau)]}\frac{\partial}{\partial\tau}h(t,\tau), \tag{A3}$$

which can be derived directly from Eq. (28) in the homogeneous gas limit.

2. Idealised pulse sequence

For simplicity, we idealise the pulse sequence in Fig. 1 by replacing the linear ramps of the first and second pulse by sudden changes of the magnetic field strength $B(t)$ at times $t_0 < t_1 < t_2 < t_3 = t_{\mathrm{final}}$, where $t_1 - t_0$ and $t_3 - t_2$ are the durations of the first and second pulse, respectively, and

$t_{\rm evolve} = t_2 - t_1$ is the evolution time. The two-body time evolution operator in Eq. (5) then factorises into the evolution operators at constant magnetic field strength:

$$U_{2\rm B}(t_3, t_0) = U_3(t_3 - t_2)U_2(t_2 - t_1)U_1(t_1 - t_0). \tag{A4}$$

The associated magnetic field strengths $B_1 = B_{\rm min} = B_3$ and $B_2 = B_{\rm evolve}$ are shown in Fig. 1. At each magnetic field strength B_i ($i = 1, 2, 3$) of the pulse sequence, the two-body Hamiltonian is stationary, and $U_i(t - t_{i-1})$ can be expanded in terms of the stationary energy states:

$$\begin{aligned} U_i(t - t_{i-1}) =& |\phi_{\rm b}(B_i)\rangle e^{-iE_{\rm b}(B_i)(t-t_{i-1})/\hbar}\langle\phi_{\rm b}(B_i)| \\ &+ \int d\mathbf{p}\, |\phi^{(+)}_{\mathbf{p}}(B_i)\rangle e^{-i\frac{p^2}{m}(t-t_{i-1})/\hbar}\langle\phi^{(+)}_{\mathbf{p}}(B_i)|. \end{aligned} \tag{A5}$$

Here $\phi_{\rm b}(B_i)$ is the the highest excited vibrational bound state whose binding energy we have denoted by $E_{\rm b}(B_i)$, and $\phi^{(+)}_{\mathbf{p}}(B_i)$ is the continuum energy state associated with the momentum $\mathbf{p}$ of the relative motion of a pair of atoms [44]. Throughout this appendix we choose the continuum wave functions to behave at asymptotically large inter-atomic distances r like

$$\phi^{(+)}_{\mathbf{p}}(\mathbf{r}) \underset{r\to\infty}{\sim} (2\pi\hbar)^{-3/2}\left[e^{i\mathbf{p}\cdot\mathbf{r}/\hbar} + f(p, \vartheta)\frac{e^{ipr/\hbar}}{r}\right], \tag{A6}$$

where $\cos\vartheta = \mathbf{p}\cdot\mathbf{r}/(pr)$ is the scattering angle, and $f(p, \vartheta)$ is referred to as the scattering amplitude. The energy associated with $\phi^{(+)}_{\mathbf{p}}(B_i)$ is given by p^2/m.

To analyse the evolution of the phase $\varphi(t)$ as well as the exponent $\gamma(t)$, we shall successively consider each period of constant magnetic field strength B_i ($i = 1, 2, 3$). The dynamic equation (A3) can be integrated from the time t_{i-1} of the previous sudden change of the magnetic field strength to the actual time t, which thus fulfils $t_{i-1} < t < t_i$. A separation of Eq. (A3) into its real and imaginary parts then yields:

$$\varphi(t) = \varphi(t_{i-1}) + \frac{1}{\hbar}\mathrm{Re}\left(\int_{t_{i-1}}^{t} dt'\, e^{2i\varphi(t')}\left[-\int_{t_{i-1}}^{\infty} d\tau\, e^{-2[\gamma(\tau)+i\varphi(\tau)]}\frac{\partial}{\partial\tau}h_i(t' - \tau) + C(t', t_{i-1})\right]\right), \tag{A7}$$

$$\gamma(t) = \gamma(t_{i-1}) - \frac{1}{\hbar}\mathrm{Im}\left(\int_{t_{i-1}}^{t} dt'\, e^{2i\varphi(t')}\left[-\int_{t_{i-1}}^{\infty} d\tau\, e^{-2[\gamma(\tau)+i\varphi(\tau)]}\frac{\partial}{\partial\tau}h_i(t' - \tau) + C(t', t_{i-1})\right]\right). \tag{A8}$$

Here $h_i(t' - \tau) = (2\pi\hbar)^3\langle 0|V(B_i)U_i(t' - \tau)|0\rangle\theta(t' - \tau)$ is the coupling function of the dynamic equation (A3) restricted to the actual period $t_{i-1} < t' < t_i$ of constant magnetic field strength B_i, and

$$C(t', t_{i-1}) = -\int_{t_0}^{t_{i-1}} d\tau\, \Psi^2(\tau)\frac{\partial}{\partial\tau}h(t', \tau) \tag{A9}$$

accounts for two-body correlations produced before the previous sudden change of the magnetic field strength at time t_{i-1}.

3. Iterative solution of the non-linear Schrödinger equation

We shall show that an approximation based on iteration of Eqs. (A7) and (A8) is sufficient to recover the essential qualitative phenomena associated with the dynamics of the atomic mean field $\Psi(t)$. We thus consider the time integrals involving the coupling function $h_i(t' - \tau)$ and the correlation term $C(t', t_{i-1})$ as a small perturbation in comparison with the initial phase $\varphi(t_{i-1})$ and the exponent $\gamma(t_{i-1})$.

The first order perturbation approximation consists in replacing, on the right hand sides of Eqs. (A7) and (A8), the phases $\varphi(t')$ and $\varphi(\tau)$ as well as the density $n_{\rm c}(\tau) = \exp(-2\gamma(\tau))$ by their initial values $\varphi(t_{i-1})$ and $n_{\rm c}(t_{i-1}) = \exp(-2\gamma(t_{i-1}))$, respectively. This procedure then shows that in the periods of constant magnetic field strength the approximate atomic mean field $\Psi(t)$ is subject to a linear time evolution

$$\Psi(t) \approx \exp\left(-\frac{i}{\hbar}\int_{t_{i-1}}^{t} dt'\, H_{\rm eff}(t', t_{i-1})\right)\Psi(t_{i-1}). \tag{A10}$$

with a complex one dimensional effective Hamiltonian

$$H_{\rm eff}(t', t_{i-1}) = n_{\rm c}(t_{i-1})h_i(t' - t_{i-1}) + e^{2i\varphi(t_{i-1})}C(t', t_{i-1}) \tag{A11}$$

This gives the following expression for the density of the atomic Bose-Einstein condensate:

$$n_{\rm c}(t) = \exp\left(\frac{2}{\hbar}\int_{t_{i-1}}^{t} dt'\, \mathrm{Im}\left[H_{\rm eff}(t', t_{i-1})\right]\right)n_{\rm c}(t_{i-1}). \tag{A12}$$

The dynamics of the condensate mean field is driven by the two-body correlations in Eq. (A9), which leads to the explicit time dependence of $H_{\rm eff}(t', t_{i-1})$. Equations (A9) and (A10) can be used to produce an iterative approximate solution of the non-linear dynamic equation (A3) for the entire pulse sequence, just on the basis of the two-body coupling function. Figure 10 shows a comparison between the dynamics of the condensate predicted by the iterative approximation and the exact solution of Eq. (A3).

The first contribution to the sum on the right hand side of Eq. (A11) provides the initially uncorrelated part of the effective Hamiltonian. Its contribution to the exponent of the atomic mean field $\Psi(t)$ in Eq. (A10) can be estimated analyti-

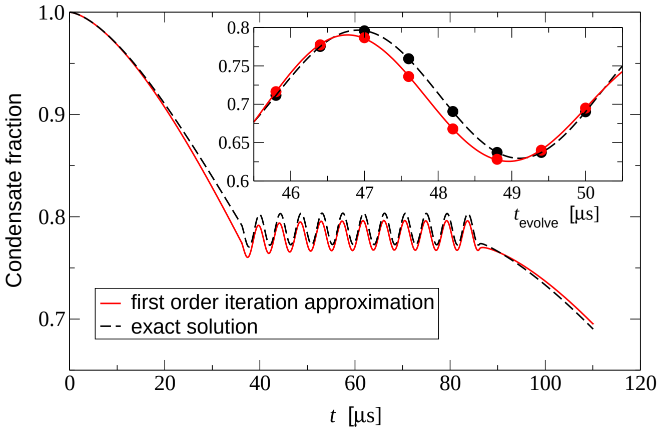

FIG. 10: Comparison between the dynamics of the atomic condensate as obtained from the exact numerical solution (dashed curve) of the non-linear Schrödinger equation (A3) and its first order iteration approximation (solid curve) for the idealised pulse sequence consisting of three periods with constant magnetic field strength. The dynamics has been determined for a magnetic field strength in the evolution period of $B_{\text{evolve}} = 160$ G, an evolution time of $t_{\text{evolve}} = 50\,\mu$s, and an initial condensate density of $n = 3.16 \times 10^{12}$ cm^{-3}. The inset shows a comparison between the Ramsey fringes in the remnant condensate as determined from the two different approaches to Eq. (A3).

cally (cf. Appendix B) from Eq. (A5) to be

$$-n_c(t_{i-1})\frac{i}{\hbar}\int_0^{t-t_{i-1}} d\tau\, h_i(\tau) = A_i(t-t_{i-1}) + D_i(t-t_{i-1}) - i\mu_i(t-t_{i-1})/\hbar \qquad \text{(A13)}$$

for each period of constant magnetic field strength B_i. Here, the leading contribution

$$\mu_i = \frac{4\pi\hbar^2}{m} n_c(t_{i-1}) a(B_i) \qquad \text{(A14)}$$

is the mean field chemical potential of the Gross-Pitaevskii equation,

$$A_i(t-t_{i-1}) = 8\pi n_c(t_{i-1}) a^3(B_i)\left[e^{-iE_b(B_i)(t-t_{i-1})/\hbar} - 1\right] \qquad \text{(A15)}$$

is an oscillating contribution associated with the bound state spectral component of Eq. (A5), and

$$D_i(t-t_{i-1}) = -4\pi n_c(t_{i-1}) a^3(B_i)\Big\{2\sqrt{i|E_b(B_i)|(t-t_{i-1})/(\pi\hbar)} - \left[1 - w\left(i\sqrt{i|E_b(B_i)|(t-t_{i-1})/\hbar}\right)\right]\Big\} \qquad \text{(A16)}$$

describes a diffusion in density and phase of the atomic mean field. The latter stems directly from the continuum part of Eq. (A5). Here, we have chosen the complex square root $\sqrt{i} = \exp(i\pi/4)$ and the function $w(z)$ denotes the complex continuation of the error function [45]:

$$w(z) = e^{-z^2}\operatorname{erfc}(-iz) = \frac{i}{\pi}\int \frac{e^{-x^2}dx}{z-x}. \qquad \text{(A17)}$$

The binding energies have been estimated in terms of the scattering length $a(B_i)$ by the universal formula $E_b(B_i) = -\hbar^2/[ma^2(B_i)]$.

The integral involving the initial correlations $C(t', t_0)$ vanishes [cf. Eq. (A9)] and Eq. (A13) is, therefore, sufficient to determine the evolution of $\Psi(t)$ during the period $t_0 < t < t_1$ of the first magnetic field pulse. In our approximate treatment the atomic mean field at the the beginning of the evolution period of the idealised pulse sequence is thus given by:

$$\Psi(t_1) = e^{A_1(t_1-t_0)+D_1(t_1-t_0)} e^{-i\mu_1(t_1-t_0)/\hbar}\Psi(t_0). \qquad \text{(A18)}$$

Moreover, since we have assumed the gas to be weakly interacting during the evolution period, it can be verified from Eqs. (A11), (A14), (A15) and (A16) that within this period of time $t_1 < t < t_2$ the atomic mean field in Eq. (A10) is well approximated by the solution

$$\Psi(t) = e^{-i\mu_2(t-t_1)/\hbar}\Psi(t_1) \qquad \text{(A19)}$$

of the Gross-Pitaevskii equation, with the initial condensate wave function $\Psi(t_1)$ given by Eq. (A18).

We shall focus in the following on the oscillatory dependence of the remnant condensate density $n_c(t_3)$ in Eq. (A12) on the evolution time $t_{\text{evolve}} = t_2 - t_1$, which determines the visibility and the frequency of the Ramsey fringes. To this end, we introduce the spectral decomposition of the two-body time evolution operator $U_2(t_2 - t_1)$ [cf. Eqs. (A4) and (A5)] in the evolution period into the, as yet undetermined, initially correlated part of the effective Hamiltonian $H_{\text{eff}}(t', t_2)$ in Eq. (A11), evaluated at times $t_2 < t' < t_3$ during the final magnetic field pulse of the sequence. A simple calculation then shows that the associated contribution to the exponent of the final atomic mean field $\Psi(t_3)$ in Eq. (A10) can be separated into high and low frequency components:

$$-\frac{i}{\hbar}\int_{t_2}^{t_3} dt\, e^{2i\varphi(t_2)} C(t, t_2) = A(t_{\text{evolve}}) + D(t_{\text{evolve}}). \qquad \text{(A20)}$$

The high frequency part, i.e.

$$A(t_{\text{evolve}}) = (2\pi\hbar)^{3/2}\langle 0|U_3(t_3-t_2)|\phi_b(B_2)\rangle e^{2i\varphi(t_2)} \times \sqrt{2}\,\Psi_b(t_1+0) e^{i|E_b(B_2)|t_{\text{evolve}}/\hbar}, \qquad \text{(A21)}$$

is associated with the spectral component of $U_2(t_2 - t_1)$ in the molecular bound state $\phi_b(B_2)$, and involves the molecular mean field [10]

$$\Psi_b(t_1+0) = -\frac{(2\pi\hbar)^{3/2}}{\sqrt{2}}\int_{t_0}^{t_1} d\tau\, \Psi^2(\tau)\frac{\partial}{\partial\tau}\langle\phi_b(B_2)|U_1(t_1-\tau)|0\rangle + \frac{(2\pi\hbar)^{3/2}}{\sqrt{2}}\Psi^2(t_1)\langle\phi_b(B_2)|0\rangle \qquad \text{(A22)}$$

at the beginning of the evolution period. Furthermore, the matrix element of $U_3(t_3 - t_2)$ on the right hand side of Eq. (A21) can be identified with the two-body probability amplitude for transitions from $|\phi_b(B_2)\rangle$ to the zero energy mode $|\phi_0\rangle = |0\rangle\sqrt{(2\pi\hbar)^3/\mathcal{V}}$ during the second, final magnetic field pulse of the sequence. The probability for the dissociation of a molecule in the bound state $\phi_{\mathrm{b}}^{\mathrm{evolve}}$ into a pair of condensate atoms during the second magnetic field pulse is given by $P_{\mathrm{b},0}^{\#2}$ [cf. Eq. (14)].

The remaining low frequency component $D(t_{\mathrm{evolve}})$ on the right hand side of Eq. (A20) involves an integral over relative momenta $\mathbf{p}$ of the amplitude associated with the burst component of the gas [10], which has evolved until the beginning of the evolution period. This diffusion part $D(t_{\mathrm{evolve}})$ is thus determined mainly by the continuum part of $U_2(t_2 - t_1)$. Its dependence on the evolution time t_{evolve} is comparatively weak. This allows us to identify the frequency as well as the visibility of the Ramsey fringes in the remnant condensate density from $A(t_{\mathrm{evolve}})$ in Eq. (A21), while $D(t_{\mathrm{evolve}})$ contributes to the average of the remnant condensate density with respect to the evolution time t_{evolve}, as well as to the small decoherence of the interference fringes. We shall focus in the following on the determination of the contributions to $A(t_{\mathrm{evolve}})$ on the right hand side of Eq. (A21).

4. Molecular mean field in the evolution period of the pulse sequence

To study the density and phase shift associated with the molecular mean field $\Psi_{\mathrm{b}}(t_1 + 0)$ in Eq. (A21), we perform a partial integration in Eq. (A22), which yields:

$$\Psi_{\mathrm{b}}(t_1 + 0) = \frac{(2\pi\hbar)^{3/2}}{\sqrt{2}} \int_{t_0}^{t_1} d\tau \, \langle \phi_{\mathrm{b}}(B_2) | U_1(t_1 - \tau) | 0 \rangle \frac{\partial}{\partial \tau} \Psi^2(\tau) + \sqrt{\frac{\mathcal{V}}{2}} \, T_{2\mathrm{B}}^{\#1}\left(\phi_{\mathrm{b}}^{\mathrm{evolve}} \leftarrow \phi_0\right) \Psi^2(t_0). \tag{A23}$$

The second contribution to the sum on the right hand side of Eq. (A23) involves the probability amplitude for the association of two asymptotically free zero energy ground state atoms into a molecular bound state $\phi_{\mathrm{b}}(B_2) = \phi_{\mathrm{b}}^{\mathrm{evolve}}$, during the first magnetic field pulse of the sequence [cf. Eq. (8)]. The first contribution, involving the time derivative of the atomic mean field, turns out to be negligible. The molecular density $n_{\mathrm{b}}^{\mathrm{evolve}} = |\Psi_{\mathrm{b}}(t_1 + 0)|^2$ then recovers the result we found using the binary classical probability theory:

$$n_{\mathrm{b}}^{\mathrm{evolve}} \mathcal{V} = N_{\mathrm{b}}^{\mathrm{evolve}} = \frac{N^2}{2} P_{0,\mathrm{b}}^{\#1}. \tag{A24}$$

Here $N = n_{\mathrm{c}}(t_0)\mathcal{V}$ and $N_{\mathrm{b}}^{\mathrm{evolve}} = n_{\mathrm{b}}^{\mathrm{evolve}}\mathcal{V}$ are the total number of atoms and the number of molecules in the evolution period, respectively, $N^2/2 \approx N(N-1)/2$ is the number of pairs of atoms in the gas, and $P_{0,\mathrm{b}}^{\#1}$ is the probability for the association of a single pair of condensate atoms with the first magnetic field pulse of the sequence to a diatomic molecule in the state $\phi_{\mathrm{b}}^{\mathrm{evolve}}$ [cf. Eq. (13)].

5. Frequency of the Ramsey fringes in the remnant condensate

In the first order iterative approximation to the non-linear Schrödinger equation (A3) the remnant condensate density $n_{\mathrm{c}}(t_3) = n_{\mathrm{c}}^{\mathrm{final}}(t_{\mathrm{evolve}})$ is determined by Eqs. (A12), (A18), (A19), and (A20) to be

$$n_{\mathrm{c}}^{\mathrm{final}}(t_{\mathrm{evolve}}) = n e^{2\mathrm{Re}[A_3(t_3-t_2)+D_3(t_3-t_2)]} e^{2\mathrm{Re}[A(t_{\mathrm{evolve}})+D(t_{\mathrm{evolve}})]} \times e^{2\mathrm{Re}[A_1(t_1-t_0)+D_1(t_1-t_0)]}, \tag{A25}$$

where $n = n_{\mathrm{c}}(t_0)$ is the total density of the gas. Since the diffusion term $D(t_{\mathrm{evolve}})$ is weakly dependent on t_{evolve}, the oscillatory amplitude $A(t_{\mathrm{evolve}})$ determines the frequency and visibility of the Ramsey interference fringes. We shall neglect the dependence of $D(t_{\mathrm{evolve}})$ on t_{evolve} in the following considerations and represent the two-body transition amplitudes of Eqs. (8) and (9) in terms of their associated probabilities and phases:

$$T_{2\mathrm{B}}^{\#1}\left(\phi_{\mathrm{b}}^{\mathrm{evolve}} \leftarrow \phi_0\right) = \left(P_{0,\mathrm{b}}^{\#1}\right)^{1/2} \exp\left(i\varphi_{0,\mathrm{b}}^{\#1}\right), \tag{A26}$$

$$T_{2\mathrm{B}}^{\#2}\left(\phi_0 \leftarrow \phi_{\mathrm{b}}^{\mathrm{evolve}}\right) = \left(P_{\mathrm{b},0}^{\#2}\right)^{1/2} \exp\left(i\varphi_{\mathrm{b},0}^{\#2}\right). \tag{A27}$$

The oscillatory amplitude $A(t_{\mathrm{evolve}})$, which provides the only contribution to the remnant condensate density in Eq. (A25) with a significant dependence on t_{evolve}, is then determined, in accordance with Eq. (A21), by:

$$A(t_{\mathrm{evolve}}) = n\mathcal{V}\left(P_{\mathrm{b},0}^{\#2} P_{0,\mathrm{b}}^{\#1}\right)^{1/2} e^{i(\omega_{\mathrm{e}} t_{\mathrm{evolve}} + \Delta\varphi - \pi/2)}. \tag{A28}$$

Here the total phase shift

$$\Delta\varphi = \pi/2 + \varphi_{0,\mathrm{b}}^{\#1} + \varphi_{\mathrm{b},0}^{\#2} + 2\left[\varphi(t_1) - \varphi(t_0)\right], \tag{A29}$$

consists of the sum of the phase shifts associated with the two-body amplitudes in Eqs. (A27) and (A26), and twice the phase shift of the atomic mean field accumulated during the first magnetic field pulse of the sequence. This can be written as

$$2\left[\varphi(t_1) - \varphi(t_0)\right] = 2\mu_1(t_1 - t_0)/\hbar - 2\mathrm{Im}\left[A_1(t_1 - t_0) + D_1(t_1 - t_0)\right]. \tag{A30}$$

We note that the amplitude $A(t_{\mathrm{evolve}})$ on the right hand side of Eq. (A28) depends just on the density of the gas rather than on its volume $\mathcal{V}$ because the product $\mathcal{V}\left(P_{\mathrm{b},0}^{\#2} P_{0,\mathrm{b}}^{\#1}\right)^{1/2}$ is independent of $\mathcal{V}$.

The angular frequency of the fringes is determined by

$$\omega_{\mathrm{e}} = \left|E_{\mathrm{b}}^{\mathrm{evolve}}\right|/\hbar + 2\left[\varphi(t_2) - \varphi(t_1)\right]/(t_2 - t_1), \tag{A31}$$

where $E_{\mathrm{b}}^{\mathrm{evolve}}$ is the binding energy of the highest excited diatomic vibrational molecular bound state, and $\varphi(t_2) - \varphi(t_1)$ is the phase shift of the atomic mean field accumulated during the evolution period. The assumption of weak interactions between the atoms during the evolution period implies that the frequency shift due to the atomic mean field can be estimated in terms of the mean field chemical potential, i.e. by

$$2\left[\varphi(t_2) - \varphi(t_1)\right]/(t_2 - t_1) \approx 2\mu_2/\hbar = 2\mu_{\mathrm{evolve}}/\hbar. \tag{A32}$$

This estimate presupposes that the contributions of Eqs. (A15) and (A16) to the phase shift have decayed during the evolution period. This stationary limit, however, is never quite reached in the experiments [8].

6. Visibility of the Ramsey fringes in the remnant condensate

Neglecting the dependence of the diffusion term $D(t_\mathrm{evolve})$ on the evolution time t_evolve in Eq. (A25), the remnant condensate density is an oscillatory function of t_evolve with maxima and minima at evolution times $t_\mathrm{evolve}^\mathrm{max}$ and $t_\mathrm{evolve}^\mathrm{min}$, which satisfy the conditions of Eqs. (16) and (17), respectively. In accordance with Eq. (A25), the visibility of the Ramsey fringes in the remnant condensate is then given by

$$V_\mathrm{Ramsey} = \frac{1-\exp\left(-2\mathrm{Re}\left[A(t_\mathrm{evolve}^\mathrm{max})-A(t_\mathrm{evolve}^\mathrm{min})\right]\right)}{1+\exp\left(-2\mathrm{Re}\left[A(t_\mathrm{evolve}^\mathrm{max})-A(t_\mathrm{evolve}^\mathrm{min})\right]\right)}, \tag{A33}$$

which leads directly to Eq. (27).

APPENDIX B: TWO-BODY TRANSITION AMPLITUDES

In this appendix we give an analytic treatment of the two-body transition amplitudes for molecular association and dissociation as well as for elastic scattering at constant magnetic field strength. These amplitudes can be used to provide estimates of the fringe visibility and the coupling function $h(t,\tau)$ of the dynamic equation (28) for the atomic mean field [cf. Eqs. (27) and (A13), respectively]. The estimates apply to an idealised pulse sequence consisting of periods of constant magnetic field strength with sudden changes in between.

1. Amplitude for elastic collisions

We first consider elastic scattering because the derivation is more concise than for molecular association or dissociation, while the basics issues are the same. In accordance with Eq. (21), the elastic transition amplitude is given by

$$\begin{aligned} T_\mathrm{2B}(\phi_0\leftarrow\phi_0) =& \langle\phi_0|U_i(t_i-t_{i-1})|\phi_0\rangle \\ \approx& 1-\frac{i}{\hbar\mathcal{V}}\int_0^{t_i-t_{i-1}} d\tau\; h_i(\tau). \end{aligned} \tag{B1}$$

This result for a constant magnetic field strength B_i ($i=1,2,3$) of an idealised pulse sequence is well approximated in terms of a coupling function $h_i(\tau)$ [cf. Eq. (20)] in the continuum limit. The derivation of Eq. (B1) takes advantage of the general formula

$$\begin{aligned} U_i(t_i-t_{i-1}) =& U_0(t_i-t_{i-1}) \\ &+\frac{1}{i\hbar}\int_{t_{i-1}}^{t_i} dt\; U_0(t_i-t)V(B_i)U_i(t-t_{i-1}), \end{aligned} \tag{B2}$$

where $U_0(t_i-t_{i-1})$ is the free time evolution operator. The latter can be expressed in terms of its spectral decomposition, i.e.

$$U_0(t_i-t_{i-1}) = \int d\mathbf{p}\; |\mathbf{p}\rangle e^{-i\frac{p^2}{m}(t_i-t_{i-1})/\hbar}\langle\mathbf{p}|. \tag{B3}$$

Here $\langle\mathbf{r}|\mathbf{p}\rangle=\exp(i\mathbf{p}\cdot\mathbf{r}/\hbar)/(2\pi\hbar)^{3/2}$ is a plane wave associated with the relative momentum $\mathbf{p}$ and with the spatial relative coordinates $\mathbf{r}$ of an atom pair.

Since the magnetic field strength is assumed to be constant in time, the time evolution operator $U_i(t-t_{i-1})$ on the right hand side of Eq. (B2) is given by the spectral representation of Eq. (A5), which determines the coupling function to be:

$$\begin{aligned} h_i(\tau) = (2\pi\hbar)^3\Bigg[\int d\mathbf{p}\;\langle 0|V(B_i)|\phi_\mathbf{p}^{(+)}(B_i)\rangle e^{-i\frac{p^2}{m}\tau/\hbar}\langle\phi_\mathbf{p}^{(+)}(B_i)|0\rangle \\ +\langle 0|V(B_i)|\phi_\mathrm{b}(B_i)\rangle e^{-iE_\mathrm{b}(B_i)\tau/\hbar}\langle\phi_\mathrm{b}(B_i)|0\rangle\Bigg]. \end{aligned} \tag{B4}$$

Here we have substituted $t-t_{i-1}=\tau$, which corresponds to the integration variable on the right hand side of Eq. (B1). We use the Lippmann-Schwinger equation [44]

$$\begin{aligned} |\phi_\mathbf{p}^{(+)}(B_i)\rangle =& |\mathbf{p}\rangle + G_0(p^2/m+i0)V(B_i)|\phi_\mathbf{p}^{(+)}(B_i)\rangle \\ =& |\mathbf{p}\rangle + G_0(p^2/m+i0)T(p^2/m+i0)|\mathbf{p}\rangle \end{aligned} \tag{B5}$$

to relate the continuum energy states of the relative motion of an atom pair $\phi_\mathbf{p}^{(+)}(B_i)$ to the energy dependent T matrix. Here

$$G_0(z) = \left(z+\hbar^2\nabla^2/m\right)^{-1} = \int d\mathbf{p}\;|\mathbf{p}\rangle\frac{1}{z-p^2/m}\langle\mathbf{p}| \tag{B6}$$

is the interaction free Green's function and "$z=p^2/m+i0$" indicates that the energy argument approaches the kinetic energy p^2/m from the upper half of the complex plane. The choice of this particular set of continuum energy states is consistent with the asymptotic behaviour of their wave functions, at large distances r between the atoms, as described by Eq. (A6).

The plane wave matrix elements of the energy dependent T matrix can be expanded in terms of the parameter $pa(B_i)/\hbar$, which to first order accuracy leads to the universal self consistent approximation

$$(2\pi\hbar)^3\langle\mathbf{p}_\mathrm{out}|T(p^2/m+i0)|\mathbf{p}_\mathrm{in}\rangle \approx \frac{4\pi\hbar^2 a(B_i)/m}{1+ipa(B_i)/\hbar}. \tag{B7}$$

We note that the incoming and outgoing momenta $\mathbf{p}_\mathrm{in}$ and $\mathbf{p}_\mathrm{out}$, respectively, do not affect the approximate result even when their associated energies p_in^2/m and p_out^2/m do not match the energy argument p^2/m of the T matrix. Equation (B7) is usually referred to as the contact potential approximation. It reflects, however, the universal low energy properties common to all T matrices, independent of the particular shape of the short range potential.

Inserting Eqs. (B5) and (B7) into Eq. (B4), the right hand side of Eq. (B1) can be represented in the form:

$$\begin{aligned} T_\mathrm{2B}(\phi_0\leftarrow\phi_0) =& 1 + A_i(t_i-t_{i-1}) + D_i(t_i-t_{i-1}) \\ &- i\mu_i(t_i-t_{i-1})/\hbar. \end{aligned} \tag{B8}$$

The last contribution on the right hand side of Eq. (B8) stems from the plane wave part of the scattering wave function in

Eq. (B5) and recovers the chemical potential μ_i of Eq. (A14), via the general relation

$$4\pi\hbar^2 a(B_i)/m = (2\pi\hbar)^3 \langle 0|V(B_i)|\phi_0^{(+)}(B_i)\rangle, \tag{B9}$$

when the volume $\mathcal{V}$ is identified with the inverse condensate density (cf. Section II).

The remaining part of the momentum integral over continuum states on the right hand side of Eq. (B4) involves complex Gaussian integrals and determines the diffusion term $D_i(t_i - t_{i-1})$. Expressed in terms of the complex error function of Eq. (A17), the diffusion term is given by

$$\begin{aligned} D_i(t_i - t_{i-1}) &= -\frac{i(2\pi\hbar)^3}{\hbar\mathcal{V}} \int_0^{t_i - t_{i-1}} d\tau \int \frac{d\mathbf{p}}{p^2/m} \left|\langle 0|V(B_i)|\phi_{\mathbf{p}}^{(+)}(B_i)\rangle\right|^2 e^{-i\frac{p^2}{m}\tau/\hbar} \\ &= -\frac{i4\pi\hbar a(B_i)}{m\mathcal{V}} \int_0^{t_i - t_{i-1}} d\tau\, w\left(i\sqrt{i|E_\mathrm{b}(B_i)|\tau/\hbar}\right) \end{aligned} \tag{B10}$$

in the contact potential approximation. Here we have used Eq. (B5) as well as the universal relation

$$E_\mathrm{b}(B_i) = -\hbar^2/\left[ma^2(B_i)\right] \tag{B11}$$

between the binding energy and the scattering length in the contact potential approximation (cf. Fig. 3). The remaining time integral on the right hand side of Eq. (B10) is readily performed using

$$\int_0^x dy\, w\left(i\sqrt{iy}\right) = i\left[1 - 2\sqrt{\frac{ix}{\pi}} - w\left(i\sqrt{ix}\right)\right], \tag{B12}$$

which leads directly to Eq. (A16).

The bound state contribution of Eq. (B8) is found from Eq. (B4) to be

$$A_i(t_i - t_{i-1}) = \frac{(2\pi\hbar)^3 |\langle 0|\phi_\mathrm{b}(B_i)\rangle|^2}{\mathcal{V}} \left[e^{-iE_\mathrm{b}(B_i)(t_i - t_{i-1})/\hbar} - 1\right], \tag{B13}$$

where we have used the momentum space Schrödinger equation

$$\langle\mathbf{p}|V(B_i)|\phi_\mathrm{b}(B_i)\rangle = \left[E_\mathrm{b}(B_i) - p^2/m\right]\langle\mathbf{p}|\phi_\mathrm{b}(B_i)\rangle \tag{B14}$$

of the bound state wave function. Inserting the universal formula

$$\phi_\mathrm{b}(r) = \frac{1}{\sqrt{2\pi a(B_i)}} \frac{e^{-r/a(B_i)}}{r} \tag{B15}$$

for the bound state wave function in the contact potential approximation into Eq. (B13) yields Eq. (A15).

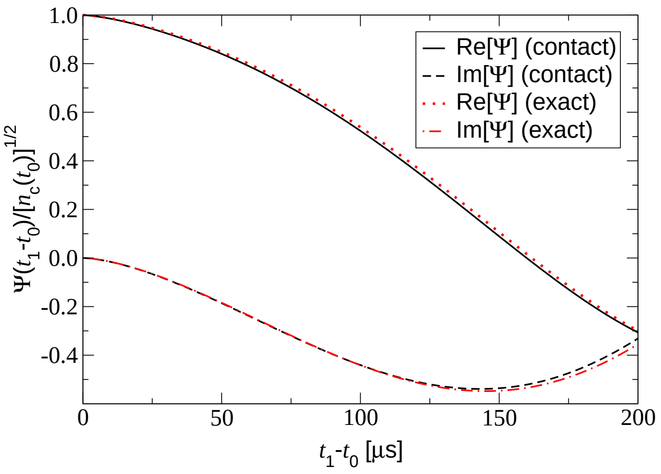

FIG. 11: Comparison between the contact potential approximation and exact numerical calculations of the two-body time evolution operator [10, 19, 20] in applications to the first order iterative approximation of the atomic mean field $\Psi(t)$ [cf. Eq. (A10)]. The numerical calculations account for the length scales set by the scattering length and by the van der Waals interaction (cf. Fig. 3). The initial condensate density of $n_\mathrm{c}(t_0) = 3.16 \times 10^{12}\,\mathrm{cm}^{-3}$ is obtained from the low density experiments of Ref. [7], while the stationary magnetic field strength of $B_1 = 155.5$ G corresponds to the typical minimum of the first pulse of the sequence in Fig. 1.

We note that in applications to time independent low energy two-body collision phenomena the contact potential approximation is valid only in a small region of magnetic field strengths in the close vicinity of the zero energy resonance, as indicated in Fig. 3. In this region the scattering length exceeds by far all the other length scales set by the inter-atomic interactions. A second restriction of the contact potential approximation, specific to the considerations in this paper, is related to the fact that dynamical phenomena involve a whole range of inter-particle collision energies E. The approximation is applicable only at low collision energies, which depend on the magnitude of the scattering length through $p_\mathrm{max} a(B_i)/\hbar \ll 1$. Here $p_\mathrm{max} = \sqrt{m|E_\mathrm{max}|}$ denotes an estimate of the maximum momentum scale set by the time evolution of the observed quantity. Figure 11 compares the contact potential approximation with exact numerical calculations [10, 19, 20] of the two-body time evolution in applications to the first order iterative approximation of the atomic mean field $\Psi(t)$ (cf. Appendix A). The comparison confirms that the approximations leading to the contact potential approach are well satisfied for the elastic transition matrix element of Eq. (B1) at the typical magnetic field strength of $B_1 = 155.5$ G during the first pulse of the sequence (cf. Fig. 1).

2. Molecular production and dissociation in magnetic field pulses

In this subsection we estimate the probabilities $P^{\#1}_{0,\mathrm{b}}$ and $P^{\#2}_{\mathrm{b},0}$, in the contact potential approximation, for idealised magnetic field pulses, which just involve sudden changes of the magnetic field strength. The derivations provide analytic estimates that reveal the sensitivity of the fringe visibilities [cf. Section II] to the shape of the magnetic field pulses. We shall consider just the amplitude $T^{\#1}_{2\mathrm{B}}(\phi_\mathrm{b}^\mathrm{evolve} \leftarrow \phi_0)$ of the first magnetic field pulse, whose time evolution operator $U_1(t_1 - t_0) = U_{\#1}(t_1, t_0)$ is translationally invariant in time, under the assumption of an idealised sequence. The second amplitude $T^{\#2}_{2\mathrm{B}}(\phi_0 \leftarrow \phi_\mathrm{b}^\mathrm{evolve})$ can then be obtained from considerations of time reversal.

As the determination of $T^{\#1}_{2\mathrm{B}}(\phi_\mathrm{b}^\mathrm{evolve} \leftarrow \phi_0)$ closely follows the considerations in the preceding section, we shall just summarise briefly the main elements of the derivation. Taking advantage of the decomposition of the time evolution operator $U_1(t_1 - t_0)$ in Eq. (B2), the transition amplitude in the continuum limit is given by:

$$T^{\#1}_{2\mathrm{B}}(\phi_\mathrm{b}^\mathrm{evolve} \leftarrow \phi_0) \approx \sqrt{\frac{(2\pi\hbar)^3}{\mathcal{V}}}\left[\langle\phi_\mathrm{b}(B_2)|0\rangle + \frac{1}{i\hbar}\int_0^{t_1-t_0} d\tau\,\langle\phi_\mathrm{b}(B_2)|U_0(t_1-t_0-\tau)V(B_1)U_1(\tau)|0\rangle\right]. \tag{B16}$$

In analogy to the derivation of the amplitude for elastic collisions, we replace the time evolution operators $U_1(\tau)$ and $U_0(t_1 - t_0 - \tau)$ by their spectral decompositions in Eqs. (A5) and (B3), respectively. The energy dependent T matrix elements that result from the continuum part of the two-body spectrum can be approximated in complete analogy to the preceding section. The momentum space bound state wave function can be determined from the Schrödinger equation (B14) to be

$$\begin{aligned}\langle\phi_\mathrm{b}(B)|\mathbf{p}\rangle &= \frac{\langle\phi_\mathrm{b}(B)|V(B)|\mathbf{p}\rangle}{E_\mathrm{b}(B) - p^2/m}\\ &\approx \frac{E_\mathrm{b}(B)}{\pi(m|E_\mathrm{b}(B)|)^{3/4}[E_\mathrm{b}(B) - p^2/m]}\end{aligned} \tag{B17}$$

in the contact potential approximation. The resulting momentum and time integrals are similar to those in the preceding section.

In the contact potential approximation, the transition amplitude of Eq. (B16) can be expressed in terms of; the scattering length $a(B_1)$ of the first magnetic field pulse, the ratio of scattering lengths

$$\gamma = a(B_2)/a(B_1) \tag{B18}$$

associated with the first magnetic field pulse and the evolution period, respectively, in addition to the phase shifts $\delta_1 = |E_\mathrm{b}(B_1)|(t_1 - t_0)/\hbar$ and $\delta_2 = |E_\mathrm{b}(B_2)|(t_1 - t_0)/\hbar$. We note that just three of these parameters can be independently varied. The final formula for the transition amplitude then reads [cf. Eq. (A17) and Ref. [45] for a discussion of the properties of the function w(z)]:

$$\begin{aligned}T^{\#1}_{2\mathrm{B}}(\phi_\mathrm{b}^\mathrm{evolve} \leftarrow \phi_0) = \sqrt{\frac{8\pi a^3(B_1)\gamma}{\mathcal{V}}}\Bigg\{&\gamma - 1 + w\left(i\sqrt{i\delta_2}\right) + \frac{2e^{i\delta_1}}{1+\gamma} + \frac{2}{1-\gamma^2}\left[\gamma w\left(i\sqrt{i\delta_1}\right) - w\left(i\sqrt{i\delta_2}\right)\right]\\ &- i\delta_2\int_0^1 dx\, w\left(i\sqrt{i\delta_2(1-x)}\right)\left[\frac{1}{\sqrt{i\pi\delta_2 x}} - w\left(i\sqrt{i\delta_2 x}\right)\right]\Bigg\}.\end{aligned} \tag{B19}$$

The application of the analytic formula of Eq. (B19) to the molecular production efficiency $P^{\#1}_{0,\mathrm{b}} = \left|T^{\#1}_{2\mathrm{B}}(\phi_\mathrm{b}^\mathrm{evolve} \leftarrow \phi_0)\right|^2$ in Fig. 12 illustrates that the contact potential approximation follows the qualitative trends of the exact numerical result. Equation (B19) clearly reveals that the efficiency of molecular production depends on the ratio $a(B_1)/[\mathcal{V}]^{1/3}$ of the length scales $a(B_1)$ set by the low energy inter-atomic interactions and the mean inter-atomic distance, respectively, on one hand (cf. Section II for a discussion of the physical meaning of the volume $\mathcal{V}$ in applications to dilute gases), and on the ratio $\gamma = a(B_2)/a(B_1)$ on the other hand. The scattering length $a(B_2)$ thereby provides an estimate of twice the mean internuclear distance [11, 31] associated with the bound state wave function $\phi_\mathrm{b}^\mathrm{evolve}$ in the evolution period. An optimal molecular production efficiency thus requires a proper balance between these length scales, which can differ by orders of magnitude under the experimental conditions of Refs. [7, 8].

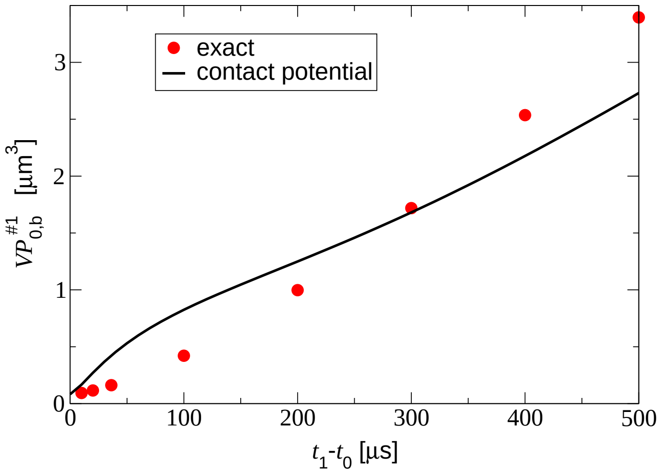

FIG. 12: The molecular production efficiency $P^{\#1}_{0,\mathrm{b}} = \left|T^{\#1}_{2\mathrm{B}}(\phi^{\mathrm{evolve}}_{\mathrm{b}} \leftarrow \phi_0)\right|^2$ as a function of the hold time $t_1 - t_0$ of the first magnetic field pulse for a minimum magnetic field strength of $B_{\mathrm{min}} = 155.5$ G (cf. Fig. 1). The magnetic field strength in the evolution period is $B_{\mathrm{evolve}} = 156.5$ G. The figure shows exact numerical calculations (filled circles) [10, 19, 20] and the contact potential approximation obtained from Eq. (B19). We note that the product $\mathcal{V}P^{\#1}_{0,\mathrm{b}}$ is independent of the volume $\mathcal{V}$.

We also note that Eq. (B19) is less accurate than Eq. (B8) for the elastic amplitude. The reason for this is mainly related to the different energy scales that enter the different amplitudes. In the case of molecular production the maximum energy scale is set by the binding energy $|E_{\mathrm{b}}(B_2)| = p^2_{\mathrm{max}}/m$ in the evolution period. The requirement $p_{\mathrm{max}}a(B_1)/\hbar \ll 1$, associated with the contact potential approximation, is violated in the applications. Studies beyond the scope of this paper show that this violation mainly affects the evolution on short time scales on the order of $t_1 - t_0 \ll \hbar/|E_{\mathrm{b}}(B_2)|$. Despite this deficit, however, the contact potential approximation provides useful qualitative insight into the dependence of the molecular production efficiency on the very different length scales set by the microscopic binary collision physics and the mean inter-atomic distance of the gas, respectively.

[1] For a review see: B. Goss Levi, Physics Today **53**, no. 9, 46 (2000).

[2] J. Herbig, T. Kraemer, M. Mark, T. Weber, C. Chin, H.-C. Nägerl, and R. Grimm, Science **301**, 1510 (2003).

[3] S. Dürr, T. Volz, A. Marte, and G. Rempe, Phys. Rev. Lett. **92**, 020406 (2004).

[4] K. Xu, T. Mukaiyama, J.R. Abo-Shaeer, J.K. Chin, D.E. Miller, and W. Ketterle, Phys. Rev. Lett. **91**, 210402 (2003).

[5] T. Mukaiyama, J.R. Abo-Shaeer, K. Xu, J.K. Chin, and W. Ketterle, Phys. Rev. Lett. **92**, 180402 (2004).

[6] S. Dürr, T. Volz, and G. Rempe, Phys. Rev. A **70**, 031601 (2004).

[7] E.A. Donley, N.R. Claussen, S.T. Thompson, and C.E. Wieman, Nature (London) **417**, 529 (2002).

[8] N.R. Claussen, S.J.J.M.F. Kokkelmans, S.T. Thompson, E.A. Donley, E. Hodby, and C.E. Wieman, Phys. Rev. A **67**, 060701 (2003).

[9] T. Köhler and K. Burnett, Phys. Rev. A **65**, 033601 (2002).

[10] T. Köhler, T. Gasenzer, and K. Burnett, Phys. Rev. A **67**, 013601 (2003).

[11] T. Köhler, T. Gasenzer, P.S. Julienne, and K. Burnett, Phys. Rev. Lett. **91**, 230401 (2003).

[12] P.D. Drummond, K.V. Kheruntsyan, and H. He, Phys. Rev. Lett. **81**, 3055 (1998).

[13] E. Timmermans, P. Tommasini, M. Hussein, and A. Kerman, Phys. Rep. **315**, 199 (1999).

[14] V.A. Yurovsky, A. Ben-Reuven, P.S. Julienne, and C.J. Williams, Phys. Rev. A **62**, 043605 (2000).

[15] A.N. Salgueiro, M.C. Nemes, M.D. Sampaio, and A.F.R.D. Piza, Physica A **290**, 4 (2001).

[16] S.K. Adhikari, J. Phys. B **34**, 4231 (2001).

[17] B.J. Cusack, T.J. Alexander, E.A. Ostrovskaya, and Y.S. Kivshar, Phys. Rev. A **65**, 013609 (2002).

[18] F.K. Abdullaev and V.V. Konotop, Phys. Rev. A **68**, 013605 (2003).

[19] T. Köhler, K. Góral, and T. Gasenzer, Phys. Rev. A **70**, 023613 (2004).

[20] K. Góral, T. Köhler, S.A. Gardiner, E. Tiesinga, and P.S. Julienne, J. Phys. B **37**, 3457 (2004).

[21] R.A. Duine and H.T.C. Stoof, Phys. Rev. Lett. **91**, 150405 (2003).

[22] Multiplying the field operator associated with the bare Feshbach resonance level [21] with the normalisation constant of the full multichannel bound state (denoted by $\sqrt{Z(B)}$ in Ref. [21]) does not change the state created (or annihilated) by it. This state is just determined by the commutation relations of the field operators [20]. Multiplying the population of the bare Feshbach resonance level with $Z(B)$ also does not in general recover the measurable fraction of dressed molecules [20] because the dressed continuum states also have a component in the bare resonance level.

[23] In the experimental reference [8], the frequency shift was attributed only to the four points closest to the zero energy resonance. For all the other experimentally investigated values of the magnetic field strentgh the shift was neglected and the associated fringe frequencies used to adjust the theoretical curve of the binding frequencies. This, in turn, determines the parameters B_0, ΔB and a_{bg}.

[24] J.L. Roberts, N.R. Claussen, S.L. Cornish, and C.E. Wieman, Phys. Rev. Lett. **85**, 728 (2000).

[25] E. Hodby, private communication.

[26] S.J.J.M.F. Kokkelmans and M.J. Holland, Phys. Rev. Lett. **89**, 180401 (2002).

[27] M. Mackie, K.-A. Suominen, and J. Javanainen, Phys. Rev.

Lett. **89**, 180403 (2002).

[28] The simulations of the remnant condensate as a function of t_{evolve} for an inhomogeneous gas in Fig. 11 of Ref. [10] were performed, by mistake, for initial conditions, which do not correspond to those reported in the caption. The strong influence of inhomogeneities reported in Subsection III D of Ref. [10] is an artifact of this mistake, and does not reflect the correct predictions of the microscopic quantum dynamics approach. Figure 2 revises Fig. 11 of Ref. [10].

[29] S.J.J.M.F. Kokkelmans, private communication.

[30] G.F. Gribakin and V.V. Flambaum, Phys. Rev. A **48**, 546 (1993).

[31] R.E. Grisenti, W. Schöllkopf, J.P. Toennies, G.C. Hegerfeldt, T. Köhler, and M. Stoll, Phys. Rev. Lett. **85**, 2284 (2000).

[32] F.H. Mies, E. Tiesinga, and P.S. Julienne, Phys. Rev. A **61**, 022721 (2000).

[33] B. Borca, D. Blume, and C.H. Greene, New J. Phys. **5**, 111 (2003).

[34] H.T.C. Stoof, A.M.L. Janssen, J.M.V.A. Koelman, and B.J. Verhaar, Phys. Rev. A **39**, 3157 (1989).

[35] J. Stenger, S. Inouye, M.R. Andrews, H.-J. Miesner, D.M. Stamper-Kurn, and W. Ketterle, Phys. Rev. Lett. **82**, 2422 (1999).

[36] B.H. Bransden and C.J. Joachain, *Physics of Atoms and Molecules* (Prentice Hall, London, 2003).

[37] P.S. Julienne, K. Burnett, Y.B. Band, and W.C. Stwalley, Phys. Rev. A **58**, 797 (1998).

[38] M.S. Child, *Molecular Collision Theory* (Academic, London, 1974).

[39] B.D. Esry, C.H. Greene and J.P. Burke, Jr., Phys. Rev. Lett. **83**, 1751 (1999).

[40] The existence of a stationary solution to the first order microscopic quantum dynamics approach of Refs. [9, 10] has been demonstrated in Ref. [19], and recovers the stationary Gross-Pitaevskii equation in the limit of weak interactions. This refutes the claim of Ref. [21] that the approach of Refs. [9, 10] can not correctly incorporate equilibrium properties.

[41] T. Köhler, E. Tiesinga, and P.S. Julienne, Phys. Rev. Lett. **94**, 020402 (2005).

[42] N.R. Claussen, E.A. Donley, S.T. Thompson, and C.E. Wieman, Phys. Rev. Lett. **89**, 010401 (2002).

[43] S.T. Thompson, E. Hodby, and C.E. Wieman, Phys. Rev. Lett. **94**, 020401 (2005).

[44] R.G. Newton, *Scattering Theory of Waves and Particles* (Springer, New York, 1982).

[45] M. Abramowitz and I.A. Stegun, *Handbook of mathematical functions* (Dover, N.Y., 1970).